



## Research paper

## 2-Anilinoquinoline based arylamides as broad spectrum anticancer agents with B-RAF<sup>V600E</sup>/C-RAF kinase inhibitory effects: Design, synthesis, *in vitro* cell-based and oncogenic kinase assessments

Ashraf K. El-Damasy<sup>a, b, \*\*</sup>, Md Mamunul Haque<sup>c</sup>, Jung Woo Park<sup>d</sup>, Sang Chul Shin<sup>e</sup>, Jun-Seok Lee<sup>c, f</sup>, Eunice EunKyeong Kim<sup>e</sup>, Gyochang Keum<sup>a, f, \*</sup>

<sup>a</sup> Center for Neuro-Medicine, Brain Science Institute, Korea Institute of Science and Technology (KIST), Hwarangro 14-gil 5, Seongbuk-gu, Seoul, 136-791, Republic of Korea

<sup>b</sup> Department of Medicinal Chemistry, Faculty of Pharmacy, Mansoura University, Mansoura, 35516, Egypt

<sup>c</sup> Molecular Recognition Research Center, KIST, Seoul, 02792, Republic of Korea

<sup>d</sup> Center for Supercomputing Applications, Div. of National Supercomputing R&D, Korea Institute of Science and Technology Information, 245, Daehak-ro, Yuseong-gu, Daejeon, 34141, Republic of Korea

<sup>e</sup> Biomedical Research Institute, KIST, Hwarangro 14-gil 5, Seongbuk-gu, Seoul, 02792, Republic of Korea

<sup>f</sup> Division of Bio-Medical Science & Technology, KIST School, Korea University of Science and Technology (UST), Seoul, 02792, Republic of Korea

## ARTICLE INFO

## Article history:

Received 17 June 2020

Received in revised form

27 July 2020

Accepted 12 August 2020

Available online 23 August 2020

## Keywords:

Anticancer activity

2-Anilinoquinoline

Arylamides

Apoptosis

Cell cycle arrest

Tubulin polymerization

B-RAF<sup>V600E</sup>

C-RAF kinase

## ABSTRACT

Prompted by the urgent demand for identification of new anticancer agents with improved potency and efficacy, a new series of arylamides incorporating the privileged 2-anilinoquinoline scaffold has been designed, synthesized, and biologically assessed. Aiming at extensive evaluation of the target compounds' potency and spectrum, a panel of 60 clinically important cancer cell lines representing nine cancer types has been used. Compounds **9a** and **9c**, with piperazine substituted phenyl ring, emerged as the most active members surpassing the anticancer potencies of the FDA-approved drug imatinib. They elicited sub-micromolar or one-digit micromolar GI<sub>50</sub> values over the majority of tested cancer cells including multidrug resistant (MDR) cells like colon HCT-15, renal TK-10 and UO-31, and ovarian NCI/ADR-RES. *In vitro* mechanistic study showed that compounds **9a** and **9c** could trigger morphological changes, apoptosis and cell cycle arrest in HCT-116 colon cancer cells. Besides, compound **9c** altered microtubule polymerization pattern in a similar fashion to paclitaxel. Kinase screening of **9c** disclosed its inhibitory activity over B-RAF<sup>V600E</sup> and C-RAF kinases with IC<sub>50</sub> values of 0.888 μM and 0.229 μM, respectively. Taken together, the current report presents compounds **9a** and **9c** as promising broad-spectrum potent anticancer candidates, which could be considered for further development of new anticancer drugs.

© 2020 Published by Elsevier Masson SAS.

## 1. Introduction

Nowadays, noncommunicable diseases including cancer are responsible for the majority of deaths over the globe [1]. Cancer

comes to the fore as the second leading cause of death worldwide, accounting for an estimated 9.6 million deaths in 2018 [2]. Among the diverse approaches for cancer prevention and treatment, chemotherapy stands as the most common therapeutic strategy [3], which involves using cytostatic or cytotoxic chemotherapeutics. Despite the remarkable benefits of the currently available chemotherapeutics, their clinical therapeutic outcomes are hampered by a narrow therapeutic index, associated undesirable adverse effects, toxicities, and emergence of drug resistance [4]. Therefore, further identification of new chemical entities with improved anticancer potency, favorable safety profile, and/or multiple mechanisms of action represents an urgent medical need [5,6].

Among the surfeit of small bioactive molecules investigated as

\* Corresponding author. Corresponding author. Center for Neuro-Medicine, Brain Science Institute, Korea Institute of Science and Technology (KIST), Hwarangro 14-gil 5, Seongbuk-gu, Seoul, 136-791, Republic of Korea.

\*\* Corresponding author. Center for Neuro-Medicine, Brain Science Institute, Korea Institute of Science and Technology (KIST), Hwarangro 14-gil 5, Seongbuk-gu, Seoul, 136-791, Republic of Korea.

E-mail addresses: [ashraf.el-damasy@kist.re.kr](mailto:ashraf.el-damasy@kist.re.kr), [ph\\_karem2000@mans.edu.eg](mailto:ph_karem2000@mans.edu.eg) (A.K. El-Damasy), [gkeum@kist.re.kr](mailto:gkeum@kist.re.kr) (G. Keum).

potential anticancer agents, arylamides are one of the privileged structural features that have attracted interest of medicinal chemists [7–16], because of their ability to modulate various molecular targets implicated in tumorigenesis. Imatinib (Gleevec®) (**I**), Fig. 1, as an example, is an arylamide Bcr-Abl kinase inhibitor that was approved by FDA for treatment of chronic myeloid leukemia (CML) [17]. Moreover, phase I and phase II studies of imatinib therapy for malignant gastrointestinal stromal tumor (GIST) showed high rates of therapeutic response [18,19]. Meanwhile, compound **II** is another arylamide derivative possessing pyrazolopyrimidine scaffold, which can overcome imatinib resistance in CML through potent inhibition of mutant Bcr-Abl<sup>T315I</sup> as well as native Bcr-Abl [20]. Furthermore, Liu *et al.* reported the identification of benzamide **III** as a selective FGFR1–3 inhibitor with potent antitumor activity against H1581 and SNU-16 xenograft models [21]. In addition, the 6,7-dimethoxyquinoline based arylamide **IV** elicited promising anticancer potency with moderate C-RAF inhibitory activity [22]. The previously described examples of anticancer arylamides **I–IV** share a common structural features involving the slim amide linker tethering a relatively bulky substituted aromatic moiety (Fig. 1, left blue-colored moieties) to a smaller aromatic fragment (Fig. 1, right green-colored fragments).

On the other hand, anilinoquinolines represent a substantial core structure for discovery of diverse active anticancer agents [23–28]. Among them, 2-anilinoquinolines, represented by compounds **V** [27] and **VI** [28] (Fig. 1), were of special interest due to

their significant broad spectrum anticancer potencies over multiple NCI cancer cell lines. Their antiproliferative activities were partially mediated by inhibition of TrkA or C-RAF kinases, with potential existence of other underlying mechanisms of action [27,28].

Molecular hybridization of two or more biologically active structural domains is a successful strategy for drug discovery in general, and for identification of novel potent anticancer agents in particular [29–33]. The hybrid molecules may offer the merits of combination therapies in a single multi-functional molecule and, therefore, be more active than conventional agents [34]. In this line and pursuing our ongoing endeavors for identification of potent anticancer agents [6,12,13,27,28], three series of 2-anilinoquinoline based arylamides, **7a–e**, **8a–e** and **9a–e**, were designed and synthesized. Our design concept was built on postulating that replacing the larger aromatic moieties of arylamides with 2-anilinoquinolines, along with conserving the amide linker joining it to the smaller aromatic fragment (Fig. 1) would generate new chemotypes with potential anticancer activity. The smaller aromatic moiety was set to be phenyl ring substituted with various groups of variable lipophilic and steric properties. Meanwhile, the amide spacer was tethered to either *meta* or *para*-position of 2-anilinoquinoline to explore the impact of amide configurations on the antiproliferative activity. The *in vitro* anticancer activities of the target molecules were evaluated against a panel of 60 clinically relevant human cancer cell lines of various types. In addition, a cell-based mechanistic study and biochemical tubulin polymerization

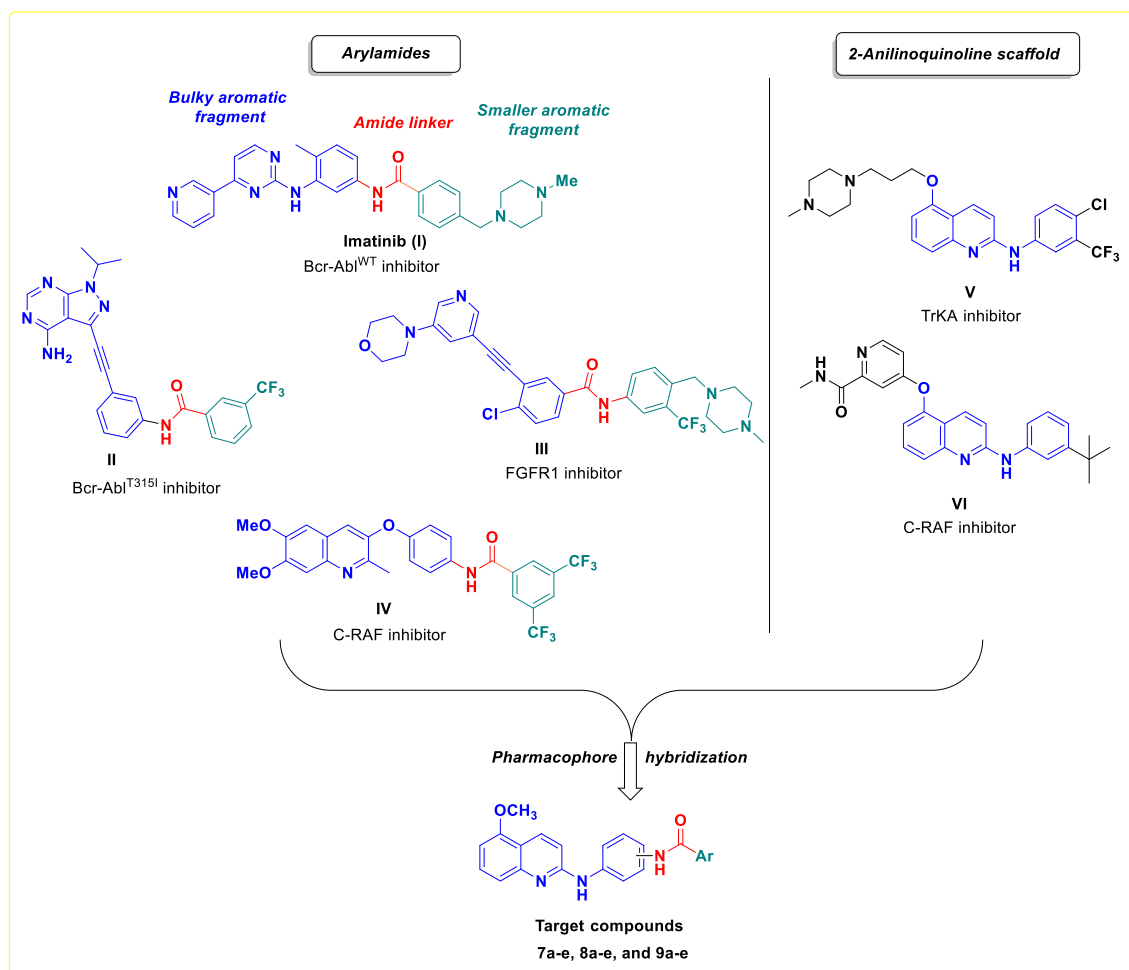


Fig. 1. Representative examples of reported anticancer arylamides and 2-anilinoquinolines, and the designed compounds.

assay for the most potent member, compound **9c**, were addressed to get insights about the possible underlying mechanism(s) for its antiproliferative activity. Furthermore, a cell-free assay of **9c** over a number of oncogenic protein kinases was examined to profile its kinase inhibitory effects and investigate the mechanism of action at molecular level.

## 2. Results and discussion

### 2.1. Chemistry

The synthetic route for preparation of the key starting material, 2-chloro-5-methoxyquinoline (**4**), is outlined in Scheme 1. *N*-Oxidation of 5-methoxyquinoline **1** was conducted using *m*-chloroperoxybenzoic acid (*m*-CPBA) in dichloromethane (DCM) to provide the corresponding *N*-oxide **2** [35]. Treatment of *N*-oxide **2** with *p*-tosyl chloride in K<sub>2</sub>CO<sub>3</sub>/DCM system afforded the lactam form of quinoline **3**, which underwent chlorination with phosphorous oxychloride to produce the 2-chloroquinoline derivative **4** in 86% yield [12,27].

As illustrated in Scheme 2, all the final compounds **7a–e**, **8a–e**, and **9a–e** were synthesized utilizing the novel intermediates, *N*<sup>1</sup>-(5-methoxyquinolin-2-yl)benzene-1,4-diamine **6a** or its 1,3-diamine isomer **6b**. The amine derivatives **6a** and **6b** were prepared, in good yield (92–95%), by nucleophilic displacement of the 2-chloroquinoline derivative **4** with *p*-nitroaniline or *m*-nitroaniline under neat condition at 160 °C for 2 h to afford the nitro anilinoquinolines **5a** and **5b**, which underwent reduction by SnCl<sub>2</sub> dihydrate and NaBH<sub>4</sub> in ethanol. Coupling of the amine **6a** or **6b** with the appropriate aryl/heteroaryl carboxylic acids in the presence of *O*-(7-azabenzotriazol-1-yl)-*N,N,N',N'*-tetramethyluronium hexafluorophosphate (HATU) and the Hünig's base (diisopropylethylamine, DIPEA) in anhydrous DMF under argon atmosphere afforded the corresponding amide derivatives **7a–e** and **8a–e**, respectively. Similarly, the cyclic amine bearing amides **9a–e** were prepared through HATU-catalyzed coupling of **6b** with various substituted 3-trifluoromethylbenzoic acid derivatives.

### 2.2. In vitro screening of the anticancer activities

#### 2.2.1. Single dose testing against NCI-60 cell line panel

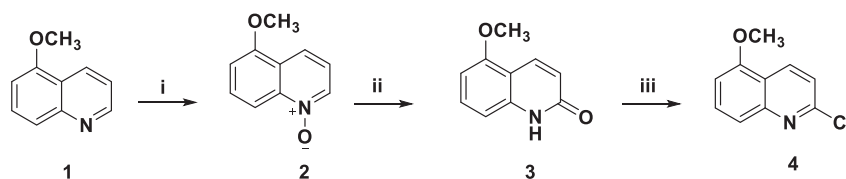
In the beginning, we synthesized the quinoline amides **7a–e** and their corresponding positional isomers **8a–e**, and their structures were submitted to National Cancer Institute (NCI, Bethesda, Maryland, USA) [36]. Out of ten derivatives, compounds **7a**, **7e** and **8a–e** were selected, based on the degree of structural variation and computer modeling techniques, for evaluation of their antiproliferative activity. The selected compounds were prescreened according to the NCI protocol at a single dose concentration of 10 μM over the full panel of approximately 60 human cancer cell lines representing nine human cancer types including; leukemia, non-small cell lung (NSCL), colon, central nervous system (CNS), melanoma, ovarian, renal, prostate, and breast tumor cell lines. The mean percentages of growth inhibition (GI) of the tested compounds across the full panel of cell lines as well as compounds' LogP

and molar refractivity (MR) are listed in Table 1. Inspection of the results revealed that anilinoquinolines substituted with arylamide at *meta* position **8a–e** are more active than the *para*-substituted derivatives **7a** and **7e**. For example, the *meta*-substituted anilinoquinolines **8a** and **8e** were more potent (mean % GI = 12.88 and 17.82, respectively) than their corresponding *para*-substituted derivatives **7a** and **7e** (mean % GI = 6.32 and –1.17, respectively), which points out the substantial nature of the attachment point between 2-anilinoquinoline scaffold and arylamide for the anticancer activity. This may be attributed to that the three carbon atoms distance (*meta*-substitution) between NH of 2-anilinoquinoline and arylamide may geometrically warrant favorable fitting of the molecule at the target active site(s). Accordingly, this would enable optimal ligand-target interactions and hence favorable anticancer activity.

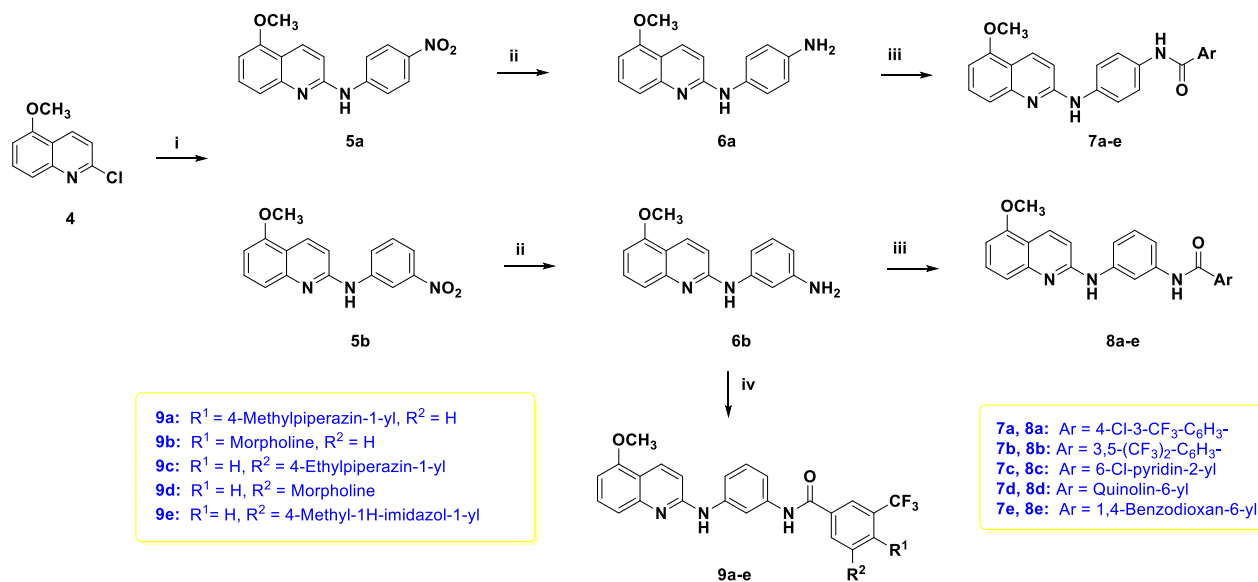
Upon correlating the observed biological activity of *meta*-substituted anilinoquinolines amides **8a–e** with their molecular descriptors LogP and molar refractivity (MR), it was found that the anticancer activity is mainly modulated by the steric factor MR rather than lipophilicity parameter LogP. The chloropyridine amide **8c** with the least MR value (111.25 cm<sup>3</sup>/mol) exerted the modest antiproliferative activity among this series (mean % GI = 4.88). In contrast, the quinolin-6-yl amide **8d** stood out as the most active member (mean % GI = 28.58) with the highest MR value of 123.00 cm<sup>3</sup>/mol. Replacing the quinoline ring of **8d** with less bulkier 1,4-benzodioxane **8e** resulted in slightly reduced anticancer activity (mean % GI = 17.82). On the other hand, the trifluoromethyl substituted derivatives **8a** and **8b** exerted comparable moderate activity with mean % GI values of 12.88 and 13.60, respectively.

Regarding the anticancer activity towards the most sensitive cancer subpanels and their susceptible cell lines (Table 2), the leukemia subpanel in general was found to be the most responsive cancer type to the tested compounds. While the *para*-substituted anilinoquinoline amide **7a** elicited moderate antileukemic activity against K-562 (GI = 47.5%) and MOLT-4 (GI = 27.6%) cell lines, all the tested *meta*-substituted derivatives **8a–e**, except **8c**, exerted significant anticancer activity (GI = 54.8–77.3%) over the same cell lines. Importantly, the multiple myeloma PRMI-8226 cell was potentially inhibited by compound **8d** (GI = 94.6%). Apart from leukemia, the prostate cancer PC-3 displayed reasonable sensitivity (GI > 50%) to compounds **8a,b** and **8d**. The most active member **8d**, with quinoline ring, exerted remarkable growth inhibitory activity towards the colon cancer cell HCT-116, renal cell 786–0, and breast cancer cell T-47D with GI values of 53.3, 51.4, and 58.0%, respectively. The full single dose screening results for compounds **7a**, **7e** and **8a–e** over all tested cell lines were inserted in the supplementary data.

As revealed from the aforementioned findings of compounds **7a–e** and **8a–e**, grafting the arylamide moiety at *meta*-position of 2-anilinoquinoline is favorable for anticancer activity. Besides, the appendage of bulky substituents with higher steric characters, MR values, at arylamide fragment seems to be essential for achieving better potency across cancer cells. Such observation lies in agreement with several reports stating that increasing the compounds' steric factor/MR values has a positive impact on augmenting their



Scheme 1. Reagents and reaction conditions: i) *m*-CPBA, DCM, 0 °C to rt, 6 h, 92%; ii) *p*-TsCl, 10% aq. K<sub>2</sub>CO<sub>3</sub>, DCM, rt, 18 h, 65%; iii) POCl<sub>3</sub>, reflux, 1 h, 86%.



**Scheme 2.** Reagents and reaction conditions: i) *m*- or *p*-Nitroaniline, neat, 160 °C, 2 h, 98% (**5a**), 96% (**5b**); ii) SnCl<sub>2</sub>·2H<sub>2</sub>O, EtOH, 90 °C, 1 h, then NaBH<sub>4</sub>, 90 °C, 0.5 h, 92% (**6a**), 95% (**6b**); iii) Aryl/heteroaryl carboxylic acid, DIPEA, HATU, DMF, rt, 18 h, 25–80%; **7e** and **8e**, 80 °C, 18 h, 62.7% (**7e**), 70.4% (**8e**); iv) 3-Trifluoromethylbenzoic acid derivative, DIPEA, HATU, DMF, rt, 2.5–4 h, 72.7–78.3%; **9c** and **9e**, 70 °C, 2.5 h, 59.3% (**9c**), 48.7% (**9e**).

**Table 1**  
Mean % growth inhibition (GI) values of compounds **7a–e** and **8a–e** over the NCI-60 cell line panel at 10 μM concentration along with their LogP and MR values.

Compound No.	Ar	Mean % GI <sup>a</sup>	LogP <sup>b</sup>	MR <sup>b</sup>
<b>7a</b>	4-Cl-3-CF <sub>3</sub> -C <sub>6</sub> H <sub>3</sub> -	6.32	6.46	119.42
<b>7b</b>	3,5-(CF <sub>3</sub> ) <sub>2</sub> -C <sub>6</sub> H <sub>3</sub> -	NT <sup>c</sup>	6.82	121.32
<b>7c</b>	6-Cl-pyridin-2-yl	NT <sup>c</sup>	4.97	111.25
<b>7d</b>	Quinolin-6-yl	NT <sup>c</sup>	5.06	123.00
<b>7e</b>	1,4-Benzodioxan-6-yl	-1.17	4.48	120.93
<b>8a</b>	4-Cl-3-CF <sub>3</sub> -C <sub>6</sub> H <sub>3</sub> -	12.88	6.46	119.42
<b>8b</b>	3,5-(CF <sub>3</sub> ) <sub>2</sub> -C <sub>6</sub> H <sub>3</sub> -	13.60	6.82	121.32
<b>8c</b>	6-Cl-pyridin-2-yl	4.88	4.97	111.25
<b>8d</b>	Quinolin-6-yl	28.58	5.06	123.00
<b>8e</b>	1,4-Benzodioxan-6-yl	17.82	4.48	120.93

<sup>a</sup> Mean % inhibition values are the averages of duplicate assays, and were calculated by dividing the summation of % inhibition values over the number of examined cell lines.

<sup>b</sup> LogP and MR (molar refractivity, cm<sup>3</sup>/mol) values were calculated by ChemDraw Professional 16.0.1 software.

<sup>c</sup> NT: Not tested.

anticancer activities [6,37–39]. In view of these considerations, and to further optimize the activity of compounds **8a–e**, a new series of anilinoquinoline based arylamides **9a–e** was designed and synthesized. We hypothesized that replacing the lipophilic chlorine of **8a** or trifluoromethyl of **8b** with bulkier cyclic amines (morpholine, 4-methyl(ethyl)piperazine) or methylimidazole (Fig. 2) might improve the compounds' steric characters as well as physico-chemical properties, and consequently the cellular potency.

The mean percentages GI of compounds **9a–e** over the NCI-60 cell lines panel, as well as compounds' LogP and MR values are shown in Table 3. As expected, all tested compounds exerted distinct superior anticancer activities (mean % GI = 32.6–95.0) to

**Table 2**  
The growth inhibition percentages of the tested compounds over the most sensitive cell lines at 10 μM concentration.<sup>a,b</sup>

Cancer type	Cell line	% Growth inhibition (GI)						
		<b>7a</b>	<b>7e</b>	<b>8a</b>	<b>8b</b>	<b>8c</b>	<b>8d</b>	<b>8e</b>
Leukemia	CCRF-CEM	–	–	32.9	34.4	–	36.9	33.4
	K-562	47.5	–	<b>56.8</b>	<b>77.3</b>	–	<b>61.1</b>	<b>67.8</b>
	MOLT-4	27.6	–	<b>54.8</b>	<b>65.2</b>	23.3	<b>64.2</b>	<b>75.2</b>
	PRMI-8226	–	–	31.8	41.9	–	<b>94.6</b>	39.7
	SR	–	–	48.0	<b>57.4</b>	–	<b>55.9</b>	<b>56.7</b>
Non-Small Cell Lung	A549/ATCC	–	–	–	48.0	–	20.9	–
	HOP-92	32	–	21.5	<b>67.5</b>	–	48.5	–
	NCI-H522	–	–	27.4	23.5	–	–	–
Colon	HCT-116	–	–	–	–	–	<b>53.3</b>	32.5
	HT29	21.8	–	–	–	–	42.4	–
Renal	786-0	–	–	–	–	–	<b>51.4</b>	48.3
	A498	22.6	–	27.5	28.6	32.4	–	26.2
	UO-31	–	–	37.6	28.2	–	22.9	–
Prostate	PC-3	–	–	<b>50.3</b>	<b>62.7</b>	20.6	<b>56.2</b>	32.1
Breast	T-47D	–	–	21.3	–	–	<b>58.0</b>	46.0

<sup>a</sup> Bold figures indicate growth inhibition > 50%.

<sup>b</sup> –; Growth inhibition <20%.

compounds **8a** and **8b**. Interestingly, the rank of compounds' antitumor activity went in direct accordance with their MR values. Piperazine derivatives **9a** (MR = 146.18) and **9c** (MR = 150.98), with the highest steric characters, emerged as the most active members with mean % GI values of 86.8 and 95.0, respectively. Next in the activity order are the two morpholines **9b** and **9d** (MR = 139.04), followed by the imidazole derivative **9e** (MR = 137.90). The overbalance of 4-methyl(ethyl)piperazine than morpholine for attaining excellent anticancer activity is a common feature among various sets of investigational anticancer compounds [6,40,41]. A possible explanation for that is that *N*-substituted piperazines are bulkier in nature and more hydrophobic than morpholine, which might enhance the hydrophobic interactions with the target proteins in cells. Or the additional terminal nitrogen of piperazine might be protonated in physiological pH, and be engaged in ionic interaction with the negatively charged carbonyl oxygen of amino acids in protein backbone, which results in strong binding affinity

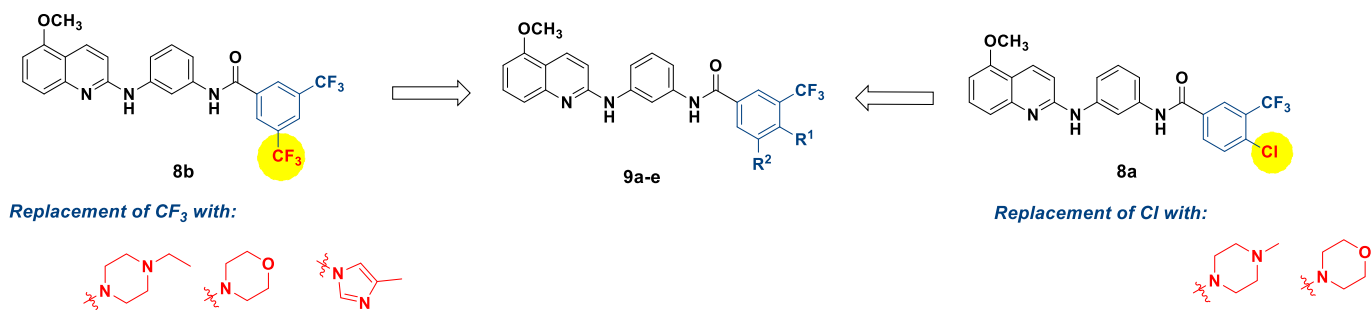
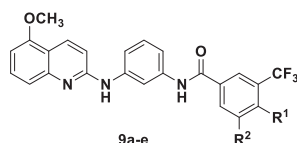


Fig. 2. Structural modifications of compounds **8a** and **8b** for optimization of their anticancer activity.

Table 3

Mean % growth inhibition (GI) values of compounds **9a–e** over the NCI-60 cell line panel at 10  $\mu$ M concentration along with their LogP and MR values.



Compound No.	R <sup>1</sup>	R <sup>2</sup>	Mean % GI <sup>a</sup>	LogP <sup>b</sup>	MR <sup>b</sup>
<b>9a</b>	4-Methylpiperazin-1-yl	H	86.8	5.94	146.18
<b>9b</b>	Morpholine	H	59.0	5.78	139.04
<b>9c</b>	H	4-Ethylpiperazin-1-yl	95.0	6.28	150.98
<b>9d</b>	H	Morpholine	38.3	5.78	139.04
<b>9e</b>	H	4-Methyl-1H-imidazol-1-yl	32.6	5.80	137.90

<sup>a</sup> Mean % inhibition values are the averages of duplicate assays, and were calculated by dividing the summation of % inhibition values over the number of examined cell lines.

<sup>b</sup> LogP and MR (molar refractivity, cm<sup>3</sup>/mol) values were calculated by ChemDraw Professional 16.0.1 software.

with the cellular target(s) [6]. Any or both of these actions, along with the enhanced compound's solubility and physicochemical characters, would allow better ligand-target binding interactions, and hence improved cellular potency. Upon comparing the activity of the two positional isomers **9b** and **9d**, it was noticed that incorporation of morpholine at 4-position next to the *m*-trifluoromethyl group (**9b**, mean % GI = 59.0) is optimal for anticancer effectiveness than 5-position (**9d**, mean % GI = 38.3). Among all of the tested derivatives, compounds **9a–c** showed the highest mean GI, and their detailed %GI over NCI-60 cell lines at concentration of 10  $\mu$ M are illustrated in Fig. 3.

Close examination of the findings illustrated in Fig. 3 unveils the broad spectrum anticancer activities of compounds **9a–c** across all the nine tested cancer subpanels. All compounds exerted strong growth inhibitory activities (>75% inhibition) over 33, 9 and 43 cell lines, respectively. The morpholine member **9b** elicited cytostatic growth inhibitory activity against multiple tumor cells, with the best activity towards HT29 colon cancer cell (%GI = 87.16). In contrast, both piperazine derivatives **9a** and **9c** exerted sound cytotoxic effects (%GI > 100) over diverse hematological and solid cancer cell lines. For example, compounds **9a** and **9c** displayed similar anticancer lethal behavior over leukemia (K-562, MOLT-4 and SR), NSCL cancer (NCI-H460 and NCI-H522), and COLO 205 and HT29 colon cancer cells. Melanoma LOX IMVI was found to be the most sensitive cancer cell towards both **9a** (%GI = 196.68) and **9c** (%GI = 194.1).

### 2.2.2. Five-dose testing

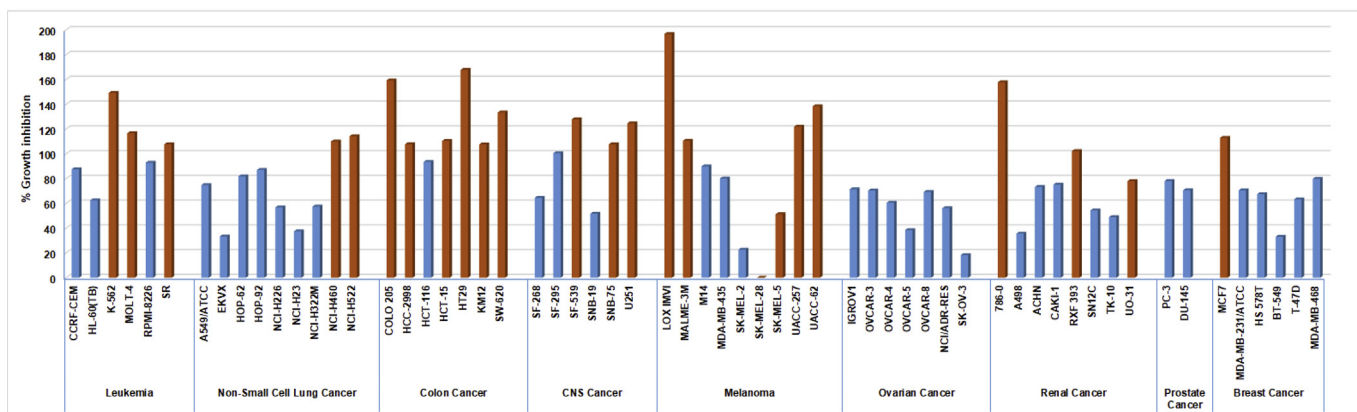
Based on the promising anticancer effects of both compounds **9a** and **9c** which fulfilled the NCI criteria for antiproliferative activity, they were further evaluated in a five-dose testing mode to determine their GI<sub>50</sub> (the molar concentration causing 50% GI), TGI (the

molar concentration producing 100% GI) and LC<sub>50</sub> (the molar concentration achieving 50% lethality or tumor regression). The GI<sub>50</sub> values, a measure of compound's potency, of **9a** and **9c** along with imatinib [42] are presented in Table 4.

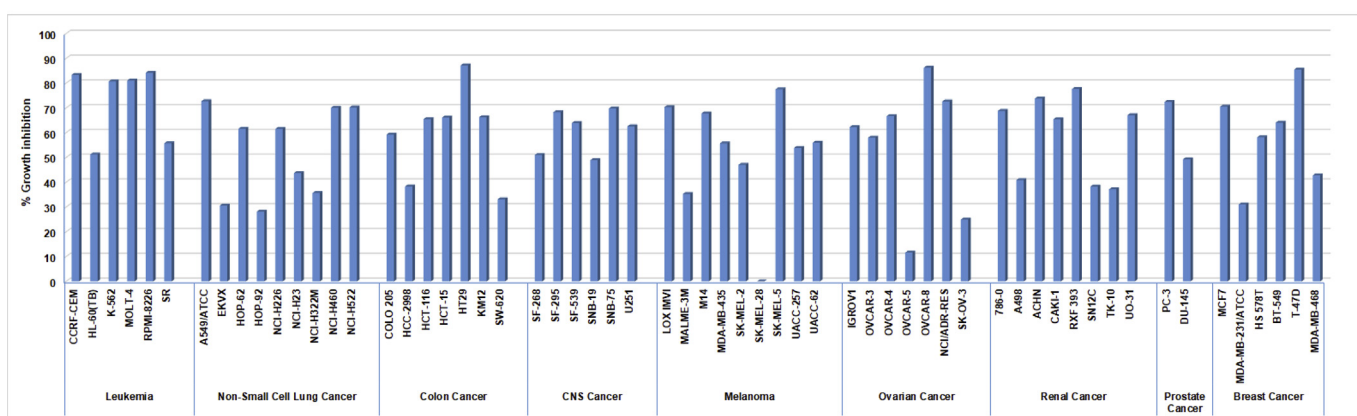
As shown in Table 4, both compounds **9a** and **9c** exerted high potency over all tested cell lines with sub-micromolar or one-digit micromolar GI<sub>50</sub> values. Interestingly, the target molecules **9a** and **9c** elicited superior potencies than imatinib against 57 cell lines. While imatinib is mainly approved for treatment of chronic myeloid leukemia (CML) [17], it is interesting to note that both **9a** and **9c** are highly potent than imatinib over four leukemia cell lines. Of special importance, compounds **9a** and **9c** showed GI<sub>50</sub> values of 0.876  $\mu$ M and 0.616  $\mu$ M against MOLT-4 cell line, being 6 and 8.3 folds more potent than imatinib, respectively. Moreover, the imatinib-irrespective lymphoma CCRF-CEM cell was potently inhibited by **9a** (GI<sub>50</sub> = 1.40  $\mu$ M) and **9c** (GI<sub>50</sub> = 0.758  $\mu$ M). Besides, the two piperazines **9a** and **9c** exhibited comparable antileukemic activity over multiple myeloma RPMI-8226 cell with GI<sub>50</sub> values of 1.65  $\mu$ M and 1.20  $\mu$ M, respectively.

On the other hand, it was reported that imatinib could improve the hypoxic conditions in non-small cell lung cancer (NSCLC) [43], as well as its ability to ameliorate drug delivery and efficacy in NSCLC xenografts [44]. In this regard, it is interesting to find that both compounds **9a** and **9c** elicited superior potency to imatinib over all nine tested NSCLC cancer cells. For instance, compounds **9a** and **9c** exerted GI<sub>50</sub> values of 0.964  $\mu$ M and 1.34  $\mu$ M against the large cell lung carcinoma cell NCI-H460 cell line, with 16.8 and 12 folds better potency than imatinib (GI<sub>50</sub> = 16.18  $\mu$ M), respectively. The methylpiperazine **9a** slightly surpassed the activity of its ethylpiperazine congener **9c** over six cells lines of NSCLC cancer panel. Compound **9a** was found to be equipotent (GI<sub>50</sub> = 0.855  $\mu$ M) over lung adenocarcinoma HOP-62 and HOP-92 cell lines.

9a



9b



9c

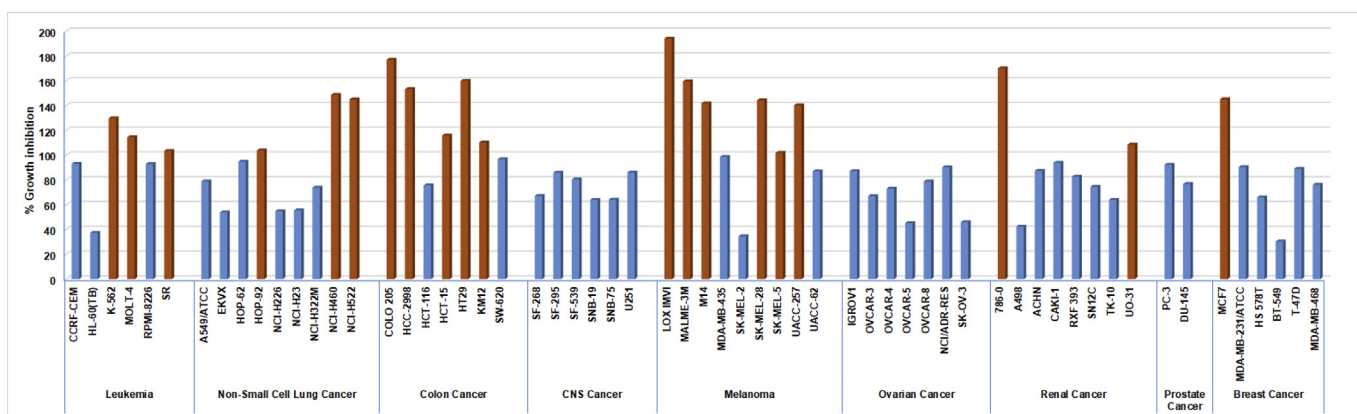


**Fig. 3.** % Growth inhibition of the 60 human cancer cell lines panel after treatment with compounds **9a–c** at 10  $\mu\text{M}$  concentration, orange colored columns refer to compound's lethal activity (%GI > 100). (For interpretation of the references to color in this figure legend, the reader is referred to the Web version of this article.)

From another perspective, imatinib has been approved for the treatment of adult patients with  $\text{KIT}^+$  (CD117) metastatic/unresectable gastrointestinal stromal tumors (GIST), and as adjuvant therapy following resection of high-risk GIST [45,46]. In this aspect, it is noteworthy mentioning that both piperazines **9a** and **9c** showed remarkable superior anticancer activities to imatinib across all colon cancer cell lines. Regarding the most imatinib-sensitive

colorectal cancer cell HT29, imatinib showed  $\text{GI}_{50}$  value of 3.97  $\mu\text{M}$ , while compounds **9a** and **9c** manifested distinct anticancer potency with  $\text{GI}_{50}$  value of 0.712  $\mu\text{M}$  and 0.572  $\mu\text{M}$ , respectively. In contrast to the two digits micromolar activity of imatinib ( $\text{GI}_{50} = 12.59\text{--}21.23 \mu\text{M}$ ) over COLO205, HCC-2998, HCT-116 and multidrug resistant (MDR) HCT-15 colon cancer cells, both compounds **9a** and **9c** showed sub-micromolar  $\text{GI}_{50}$  values

**Table 4**  
GI<sub>50</sub> values (μM) of **9a**, **9c** and imatinib over NCI-60 cell line panel.<sup>a,b,c</sup>

Cell lines	GI <sub>50</sub> (μM)			Cell lines	GI <sub>50</sub> (μM)		
	<b>9a</b>	<b>9c</b>	Imatinib		<b>9a</b>	<b>9c</b>	Imatinib
<b>Leukemia</b>				M14	<b>0.899</b>	<b>0.668</b>	19.28
CCRF-CEM	1.40	<b>0.758</b>	16.98	MDA-MB-435	<b>0.878</b>	1.16	17.91
HL-60(TB)	1.07	3.82	13.49	SK-MEL-2	1.36	5.30	25.00
K-562	1.10	<b>0.910</b>	<b>0.02</b>	SK-MEL-28	<b>0.896</b>	<b>0.846</b>	14.62
MOLT-4	<b>0.876</b>	0.616	5.13	SK-MEL-5	1.52	1.55	12.13
RPMI-8226	1.65	1.20	6.05	UACC-257	1.36	1.02	21.13
SR	1.13	0.883	7.14	UACC-62	1.06	1.50	19.01
<b>Non-Small Cell Lung Cancer</b>				<b>Ovarian Cancer</b>			
A549/ATCC	1.43	1.05	24.49	IGROV1	1.25	<b>0.924</b>	21.18
EKVX	1.83	3.07	26.18	OVCAR-3	1.21	3.41	34.20
HOP-62	<b>0.856</b>	1.02	21.53	OVCAR-4	1.43	1.57	20.04
HOP-92	<b>0.854</b>	1.26	13.34	OVCAR-5	1.53	2.78	<b>0.58</b>
NCI-H226	2.26	2.85	18.11	OVCAR-8	1.69	1.97	27.67
NCI-H23	2.93	3.41	14.96	NCI/ADR-RES	1.50	1.29	22.96
NCI-H322M	1.65	1.33	22.80	SK-OV-3	1.73	4.60	28.91
NCI-H460	<b>0.964</b>	1.34	16.18	<b>Renal Cancer</b>			
NCI-H522	1.04	1.01	16.41	786-0	0.923	3.73	16.00
<b>Colon Cancer</b>				A498	1.80	4.94	21.98
COLO 205	<b>0.909</b>	<b>0.654</b>	17.62	ACHN	1.53	1.21	25.23
HCC-2998	<b>0.950</b>	<b>0.720</b>	21.23	CAKI-1	1.12	<b>0.917</b>	33.96
HCT-116	<b>0.868</b>	<b>0.872</b>	12.59	RXF 393	<b>0.802</b>	<b>0.918</b>	15.07
HCT-15	<b>0.937</b>	<b>0.798</b>	19.95	SN12C	1.7	1.39	33.19
HT29	<b>0.712</b>	<b>0.572</b>	3.97	TK-10	2.01	3.47	26.85
KM12	1.09	1.71	18.84	UO-31	<b>0.734</b>	<b>0.746</b>	22.34
SW-620	<b>0.968</b>	3.67	23.44	<b>Prostate Cancer</b>			
<b>CNS Cancer</b>				PC-3	1.26	0.805	21.38
SF-268	1.50	1.76	26.30	DU-145	1.81	1.88	18.79
SF-295	<b>0.967</b>	<b>0.803</b>	19.77	<b>Breast Cancer</b>			
SF-539	<b>0.895</b>	3.28	10.57	MCF7	<b>0.851</b>	<b>0.679</b>	18.24
SNB-19	1.11	2.10	38.55	MDA-MB-231	1.55	1.80	18.66
SNB-75	<b>0.695</b>	1.05	20.28	HS 578T	1.07	3.61	14.59
U251	<b>0.885</b>	1.36	17.99	BT-549	2.79	3.78	16.11
<b>Melanoma</b>				T-47D	1.00	2.05	19.91
LOX IMVI	<b>0.873</b>	<b>0.780</b>	18.11	MDA-MB-468	1.11	<b>0.749</b>	NT <sup>c</sup>
MALME-3M	<b>0.816</b>	<b>0.611</b>	16.33				

<sup>a</sup> Data were obtained from the National Cancer Institute (NCI) in vitro disease-oriented human tumor cell line screen (five-dose–response curve) for compounds **9a** (NSC 806983), **9c** (NSC 806531), and imatinib (NSC 759854).

<sup>b</sup> Bold figures refer to sub-micromolar GI<sub>50</sub> values.

<sup>c</sup> NT: Not tested.

spanning in the range of 0.654–0.950 μM. Such potent cellular outcomes nominate **9a** and **9c** for further investigations as potential therapeutics for colorectal cancer.

While most of tyrosine kinase inhibitors including imatinib are ineffective in glioblastoma (GBM) [47,48], the most intractable type of brain cancers [49], compounds **9a** and **9c** were significantly superior to imatinib over all six tested brain cancer cell lines. In addition, **9a** and **9c** displayed considerable potencies against the temozolomide (TMZ)-resistant cell lines SF-295, SNB-75, SNB-19 and SF-268 gliomas. The methylpiperazine member **9a** was the most potent member towards SNB-75 cell line (GI<sub>50</sub> = 0.695 μM), whereas ethylpiperazine **9c** showed the best activity against SF-295 cell line (GI<sub>50</sub> = 0.803 μM).

Despite the FDA approved diarylamide imatinib has modest anticancer activity against diverse melanoma cells, the 2-anilinoquinoline based arylamides **9a** and **9c** elicited potent anticancer activity against all tested melanoma cell lines, with sub-micromolar activity over LOX IMVI, MALME-3M, M14, and SK-MEL-28. For example, **9c** exhibited nanomolar GI<sub>50</sub> values of 611 nM, 668 nM, and 846 nM over MALME-3M, M14, and SK-MEL-28 cell lines, respectively. Furthermore, both compounds **9a** and **9c** showed equipotent activity (GI<sub>50</sub> = 1.54 μM) against SK-MEL-5 cell line.

Moreover, imatinib was investigated for treatment of certain ovarian cancers, and showed significant clinical therapeutic

benefits especially in combination with other chemotherapeutic agents like docetaxel [50,51]. In this regard, it is noteworthy mentioning that compounds **9a** and **9c** possess significant anti-proliferative activity surpassing imatinib against all tested ovarian cancer cells, except OVCAR-5. Compound **9c** exhibited nanomolar GI<sub>50</sub> values of 924 nM over IGROV1 cell line. Furthermore, **9a** and **9c** showed equipotent activity (GI<sub>50</sub> = 1.5 μM) against the OVCAR-4 cell line, being 13 folds more potent than imatinib (GI<sub>50</sub> = 20.04 μM). Of special interest, both piperazines **9a** and **9c** elicited excellent potency over the paclitaxel-resistant NCI/ADR-RES cell line, with GI<sub>50</sub> values of 1.50 μM and 1.29 μM, respectively.

In addition to the aforementioned targeted cellular potencies of compounds **9a** and **9c**, they displayed broad spectrum potencies over numerous cell lines of different cancer types. The RXF 393 and MDR UO-31 renal cells were highly sensitive to both compounds **9a** (GI<sub>50</sub> = 0.802 μM and 0.734 μM) and **9c** (GI<sub>50</sub> = 0.918 μM and 0.746 μM), respectively. Moreover, the ACHN, CAKI-1, and SN12C renal cancer cell lines were responsive to compounds **9a** and **9c** (GI<sub>50</sub> values of 0.917–1.7 μM). Furthermore, both **9a** and **9c** exerted potent antiproliferative effects against MCF7 breast cancer cell line with GI<sub>50</sub> values of 851 nM and 679 nM, respectively. Besides, the ethylpiperazine member **9c** elicited pronounced anticancer activities over the prostate cancer cell PC-3 and triple negative breast cancer cell MDA-MB-468 with GI<sub>50</sub> values of 0.805 μM and 0.749 μM, respectively.

Upon comparing the anticancer potency of the newly identified chemotypes **9a** and **9c** with the previously reported quinoline derivative **IV** (Table 5), it was obvious that compounds **9a** and **9c** are more potent than **IV** over most of the examined cell lines. For example, compound **9c** showed equipotent potency against SF-295 CNS cancer and PC-3 prostate cancer cell lines (GI<sub>50</sub> = 0.804 μM), with two folds improved potency than **IV** (GI<sub>50</sub> = 1.65 μM). Moreover, compound **9a** elicited three folds superior anticancer potency (GI<sub>50</sub> = 1.43 μM) to **IV** (GI<sub>50</sub> = 4.53 μM) over OVCAR-4 ovarian cancer cell line.

In view of the efficacy parameters (TGI and LC<sub>50</sub> values) of compounds **9a** and **9c** (Table 6), it was obvious that both **9a** and **9c** are of comparable efficacy (TGI < 5.0 μM) across a number of the examined cancer cells, whereas the methylpiperazine **9a** showed relatively better efficacy than its corresponding ethylpiperazine **9c** in terms of LC<sub>50</sub> < 10.0 μM. Noticeably, **9a** proved to be highly efficacious towards the LOX IMVI melanoma cell with TGI and LC<sub>50</sub> values of 1.57 μM and 2.83 μM, respectively. Moreover, **9c** showed the best efficacy against HT29 colon cancer cell with TGI and LC<sub>50</sub> values of 1.21 μM and 2.56 μM, respectively.

### 2.3. Cytotoxicity test against L132 and Vero normal cells

To acquire insights about the selective cytotoxicity of this new series of 2-anilinoquinolines, the most potent derivatives **9a** and **9c** have been tested against two normal cells from different origins (L132; derived from human embryonic lung, and Vero; derived from adult green monkey kidney) (Table 7). Interestingly, both compounds **9a** and **9c** displayed low cytotoxic activities, as indicated by the high cell viability %, at the examined doses of 1–10 μM. Such outcomes point out the differential cytotoxic effects of **9a** and **9c** towards cancer cells rather normal cell lines.

### 2.4. In vitro cell-based mechanistic studies

#### 2.4.1. Apoptotic nuclear chromatin analysis by Hoechst staining

Hoechst is a blue-fluorescent dye that typically binds to DNA, and stains the DNA in apoptotic cells more brightly than the normal cells providing information about the cells' nuclei in terms of shape and density. Accordingly, we used Hoechst stain to investigate the

**Table 5**  
GI<sub>50</sub> values (μM) of **9a**, **9c** and the reported quinoline **IV** over selected cancer cell lines.<sup>a</sup>

Compound No.	Cancer cell lines, GI <sub>50</sub> values (μM)								
	RPMI-8226	HOP-92	HCT-116	SF-295	SK-MEL-5	OVCAR-4	A498	PC-3	BT-549
<b>9a</b>	1.65	<b>0.854</b>	<b>0.868</b>	<b>0.967</b>	<b>1.52</b>	<b>1.43</b>	1.80	<b>1.26</b>	<b>2.79</b>
<b>9c</b>	<b>1.20</b>	<b>1.26</b>	<b>0.872</b>	<b>0.803</b>	<b>1.55</b>	<b>1.57</b>	4.94	<b>0.805</b>	3.78
<b>IV</b> <sup>b</sup>	1.57	1.82	1.56	1.64	2.76	4.53	1.13	1.66	3.02

<sup>a</sup> Data of compounds **9a** and **9c** are taken from Table 4, and bold figures indicate superior potency to the reported quinoline **IV**.

<sup>b</sup> Reported data [22].

**Table 6**  
TGI and LC<sub>50</sub> values (μM) of compounds **9a** and **9c** over the most sensitive cell lines.<sup>a</sup>

Cancer type	Cell line	<b>9a</b>		<b>9c</b>	
		TGI	LC <sub>50</sub>	TGI	LC <sub>50</sub>
Leukemia	CCRF-CEM	>50.0	>50.0	<b>2.06</b>	<u>8.04</u>
	PRMI-8226	6.44	>50.0	5.32	15.3
NSCL	HOP-92	<b>4.03</b>	18.8	<b>4.66</b>	16.6
Colon	HCT-116	<b>1.89</b>	<u>4.10</u>	<b>3.54</b>	12.4
	HT29	<b>1.61</b>	<u>3.65</u>	<b>1.21</b>	<u>2.56</u>
CNS	SF-295	<b>1.92</b>	<u>3.82</u>	<b>2.25</b>	11.4
Melanoma	LOX IMVI	<b>1.57</b>	<u>2.83</u>	<b>1.96</b>	<u>7.04</u>
	MALME-3M	<b>1.62</b>	<u>3.20</u>	<b>1.33</b>	<u>2.88</u>
	M14	<b>1.95</b>	<u>4.21</u>	<b>1.65</b>	<u>5.86</u>
Ovarian	IGROV1	<b>4.24</b>	25.6	5.23	20.0
Renal	UO-31	<b>1.49</b>	<u>3.04</u>	<b>3.88</b>	12.4
Breast	MCF7	<b>1.90</b>	<u>4.25</u>	<b>2.28</b>	17.6
	MDA-MB-468	<b>3.65</b>	18.4	<b>4.05</b>	14.6

<sup>a</sup> Bold figures refer to TGI values less than 5 μM, and underlined figures indicate LC<sub>50</sub> less than 10 μM.

**Table 7**  
Cytotoxicity evaluation of compounds **9a** and **9c** against L132 and Vero normal cell lines.<sup>a</sup>

Compound No.	Tested concentrations	Cell viability (%)	
		L132	Vero
<b>9a</b>	1 μM	97.03 ± 0.11	86.52 ± 0.05
	3 μM	88.57 ± 0.04	86.93 ± 0.03
	10 μM	66.07 ± 0.13	77.13 ± 0.08
<b>9c</b>	1 μM	91.24 ± 0.01	81.48 ± 0.02
	3 μM	82.83 ± 0.01	76.75 ± 0.03
	10 μM	68.19 ± 0.01	74.08 ± 0.02

<sup>a</sup> The presented values are the means of two experiments ± SEM.

nuclear damage and morphological changes which occur upon apoptosis induction or DNA damage in cancer cells. After treatment of HCT-116 colon cancer cells with compounds **9a** and **9c**, the cells began to exhibit significant apoptotic events such as cell shrinkage, nuclear condensation and fragmentation. It was evident that bright blue spots became denser upon increasing compounds' concentration and incubation time, revealing that compounds **9a** and **9c** induced apoptosis in the HCT-116 cells in both dose and time-dependent manner (Fig. 4).

#### 2.4.2. Cell cycle effects

To get certain insights about the underlying mechanism(s) of anticancer activity triggered by compounds **9a** and **9c**, their effects on cell cycle dynamics of HCT-116 colon cancer cell line were evaluated. The cell cycle distribution was analyzed, by flow cytometry, after treatment of HCT-116 cells with 1.25 μM, 2.5 μM and 5 μM concentrations of compounds **9a** and **9c** for 24 h or 48 h (Fig. 5). As shown in Fig. 5 and Table 8, both **9a** and **9c** induced cell cycle arrest of HCT-116 cells at G0/G1 phase in a dose-dependent manner, as well as a certain increase in sub-G1 phase which indicates the apoptotic activity of **9a** and **9c**. For example, the

population of HCT-116 cells at G0/G1 phase was increased from 65.0% (control) to 69.7% and 71% after treatment with 2.5 μM and 5 μM doses of **9a** for 24 h, respectively. Similarly, treatment of HCT-116 cells with increasing concentrations of **9c** for 48 h was associated with remarkable accumulation of cells at G0/G1 phase, as well as reduction of cell count at G2/M phase. Such cell-based outcomes strongly suggest the ability of compounds **9a** and **9c** to induce cell cycle perturbations in cancer cells.

#### 2.4.3. Induction of apoptosis in cancer cells

In order to further confirm the pro-apoptotic activity of compounds **9a** and **9c** in cancer cells, the Annexin V and PI staining were undertaken using HCT-116 colon cancer cells. Flow cytometry analysis of stained cells can distinguish cells into four categories, namely viable (LL: Annexin V-negative/PI-negative), early apoptosis (LR: Annexin V-positive/PI-negative), late apoptosis (UR: Annexin V-positive/PI-positive) and necrotic cells (UL: Annexin V-negative/PI-positive). Referring to the obtained data (Fig. 6), it was found that the treatment of HCT-116 cells with **9a** and **9c** was associated with an increase in the early apoptotic populations in both a dose and time-dependent manner. For example, while the population of early apoptotic cells was 7.7% in control (48 h), their populations were 16.6%, 19.0% and 26.8% after treatment with 1.25 μM, 2.5 μM and 5.0 μM concentrations of **9c** for 48 h.

#### 2.5. Tubulin polymerization assay

As a part of our mechanistic study for compounds **9a** and **9c**; their potential effects on tubulin polymerization were investigated (Fig. 7). While the methylpiperazine derivative **9a** showed minimal effect on microtubule polymerization, the most potent member **9c** exerted significant increase in microtubule polymerization in a similar fashion to the well-known microtubule stabilizing agent paclitaxel. Such findings suggest the tubulin binding activity of **9c** as an additional mechanism of action, which might contribute to its potent and broad spectrum anticancer activity.

#### 2.6. In vitro kinase screening

In attempt to investigate the mechanism of action and the kinase inhibitory profile of this novel array of 2-anilinoquinoline based arylamides, the most potent member **9c** was tested over a panel of 20 cancer relevant kinases at 10 μM concentration at Reaction Biology Corporation (RBC, Malvern, PA, USA) [52]. As depicted in Fig. 8, compound **9c** exerted high Pan-RAF kinase inhibitory activity against B-RAF<sup>wild</sup>, B-RAF<sup>V600E</sup>, and C-RAF (RAF1) with 94.40–97.66% inhibition. It is noteworthy mentioning that the RAF-inhibitory activity of **9c** is significantly superior to that of the previously reported quinoline amide **IV**. At the same tested dose, 10 μM, compound **IV** exerted 76.65% inhibition against C-RAF, and less than 47% inhibition against B-RAF<sup>wild</sup> and B-RAF<sup>V600E</sup> kinases [22]. Moreover, the receptor tyrosine kinases DDR1 and TrKA were significantly suppressed by **9c** with 94.45% and 87.98% inhibition,

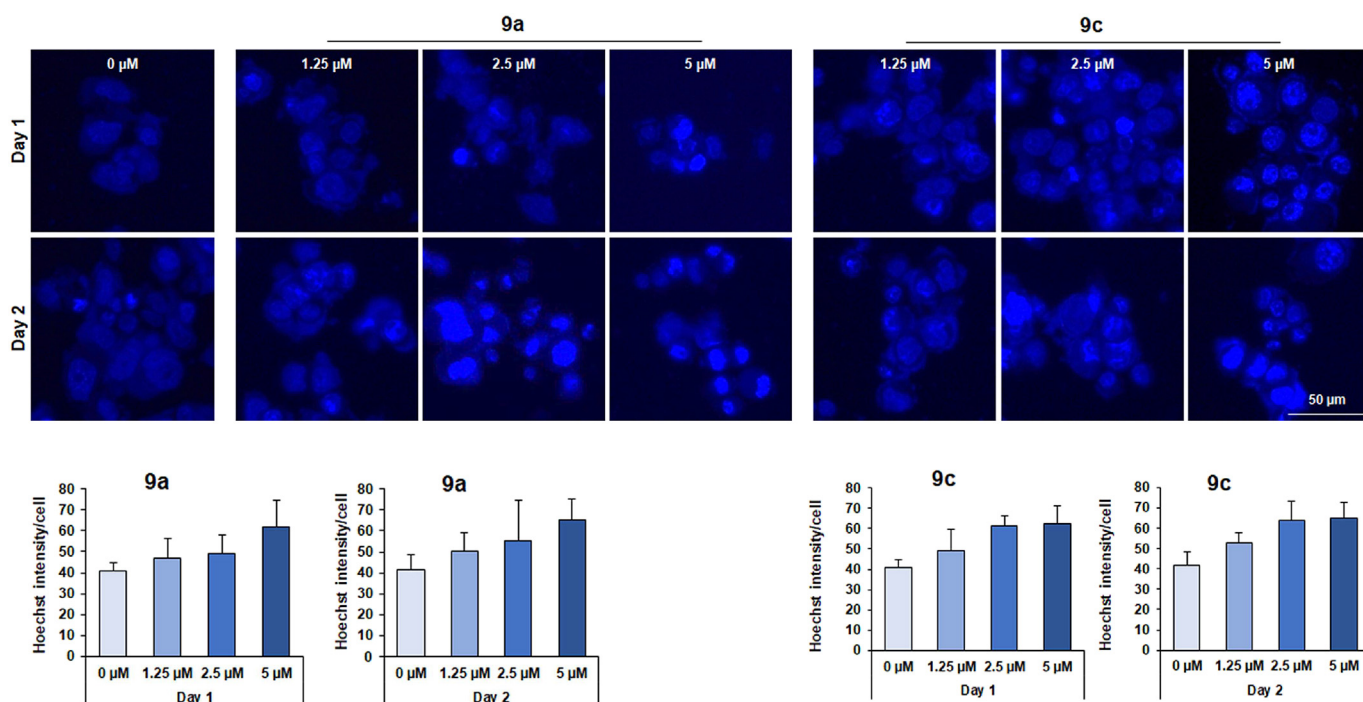


**Fig. 4.** Morphological changes (Hoechst staining) in HCT-116 cells induced by compounds **9a** and **9c** after 24 h and 48 h. The cells were treated with compounds **9a** and **9c** at different concentrations and different time-intervals followed by Hoechst staining and imaging, and the scale bar is 50  $\mu\text{m}$ . The bar graph represents the mean fluorescence intensity of the cells (R.F.U.).

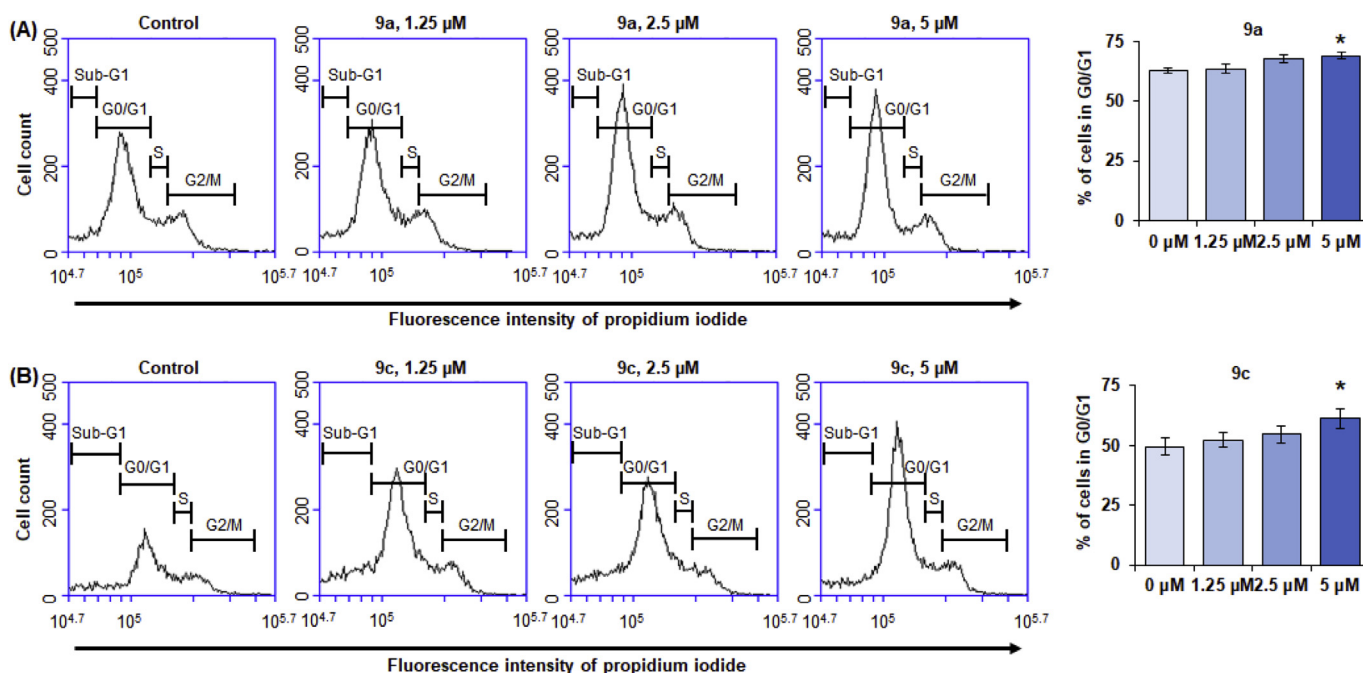


**Fig. 5.** Flow cytometric analysis of HCT-116 cell cycle after treatment with different concentrations of compounds **9a** (A) and **9c** (B) and incubation for 24 h and 48 h, respectively. The histograms show the representative plots of the experiment, and the bar graphs represent the mean of G0/G1 phase from two different experiments. \* indicates  $p < 0.05$ .

respectively. Meanwhile, it showed moderate activity over DDR2 (67.52% inhibition) and FMS (60.68% inhibition), as well as modest activity towards the other kinases with inhibition percentage less than 50. Accordingly, the most cell potent members **9a** and **9c** were further tested in a 10-dose testing mode to determine their  $\text{IC}_{50}$  values over the top three sensitive kinases C-RAF, DDR1, and TrKA

(Table 9). The ethylpiperazine derivative **9c** elicited superior potency to its methylpiperazine congener **9a** against all three tested kinases. Of particular significance, **9c** (DDR1;  $\text{IC}_{50} = 0.538 \mu\text{M}$ , TrKA;  $\text{IC}_{50} = 1.67 \mu\text{M}$ ) showed 4 and 20 folds outperformed activity than **9a** (DDR1;  $\text{IC}_{50} = 2.25 \mu\text{M}$ , TrKA;  $\text{IC}_{50} = 34.0 \mu\text{M}$ ) towards DDR1 and TrKA kinases, respectively. On the other hand, both **9a**

**Table 8**  
Cell cycle distribution of HCT-116 cell line treated with **9a** and **9c**.<sup>a</sup>

<b>9a</b> (conc.)	% of cell cycle phases' distribution (24 h)				<b>9c</b> (conc.)	% of cell cycle phases' distribution (48 h)			
	Sub-G1	G1/G0	S	G2/M		Sub-G1	G1/G0	S	G2/M
0 $\mu$ M	8.7	65.0	7.2	19.2	0 $\mu$ M	17.0	52.2	10.4	20.4
1.25 $\mu$ M	9.6	66.6	8.2	15.6	1.25 $\mu$ M	21.0	54.7	8.8	15.5
2.5 $\mu$ M	7.9	69.7	7.3	15.1	2.5 $\mu$ M	20.9	57.1	9.2	12.9
5.0 $\mu$ M	9.1	71.0	6.3	13.7	5.0 $\mu$ M	14.1	64.1	7.4	14.4

<sup>a</sup> Flow cytometric analysis of HCT-116 cell cycle was performed after incubation with compounds **9a** and **9c** for 24 h and 48 h, respectively.

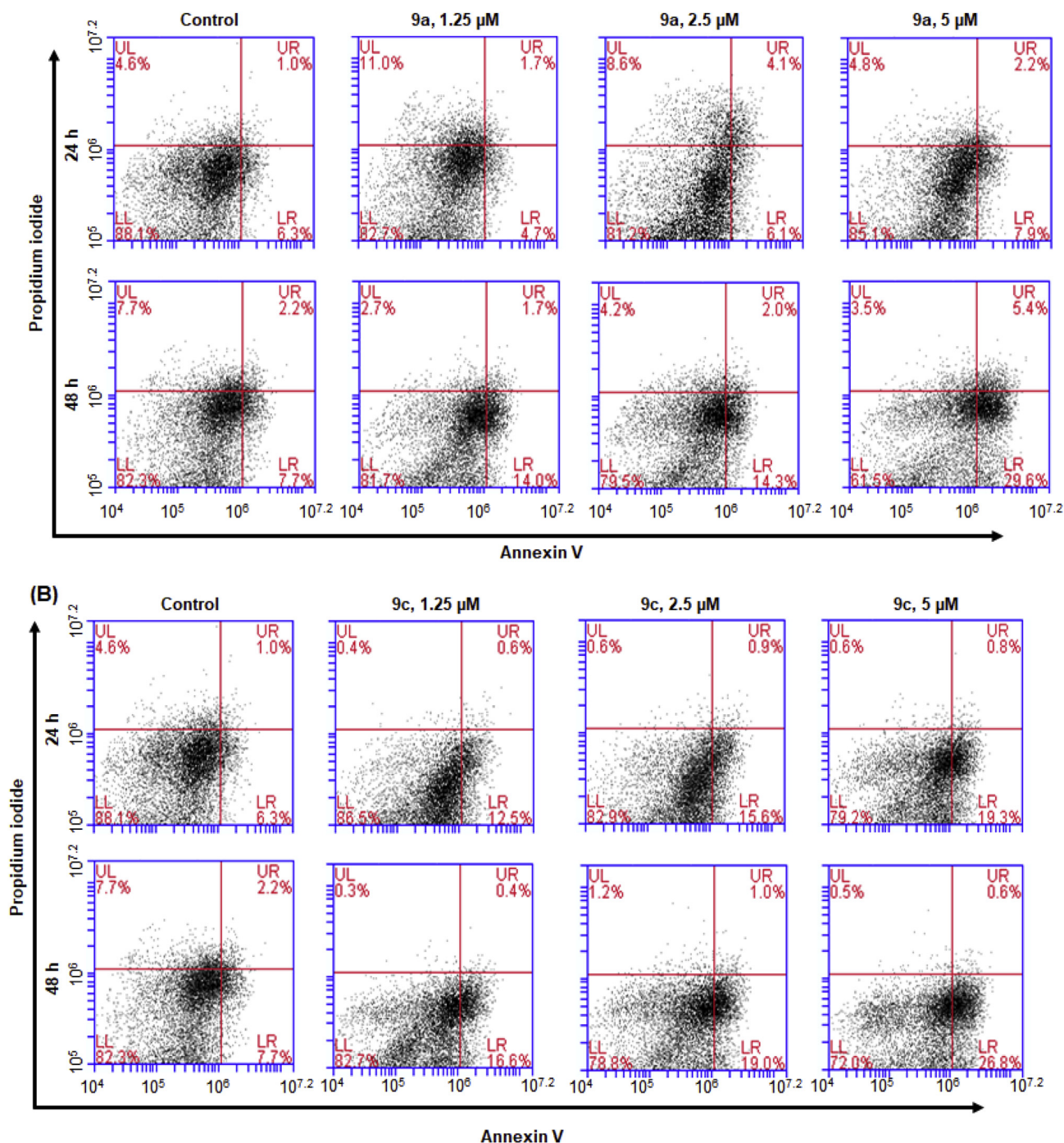


**Fig. 6.** Characterization of HCT-116 apoptosis after being treated with compounds **9a** (A) and **9c** (B) for 24 h and 48 h, as determined by Annexin V and PI staining. Quadrants were defined as LR = early-stage apoptosis (Annexin V-negative/PI-negative) and UR = late-stage apoptosis (Annexin V-positive/PI-positive). Histogram showed percentages of early apoptotic and late apoptotic cells after 24 h and 48 h.

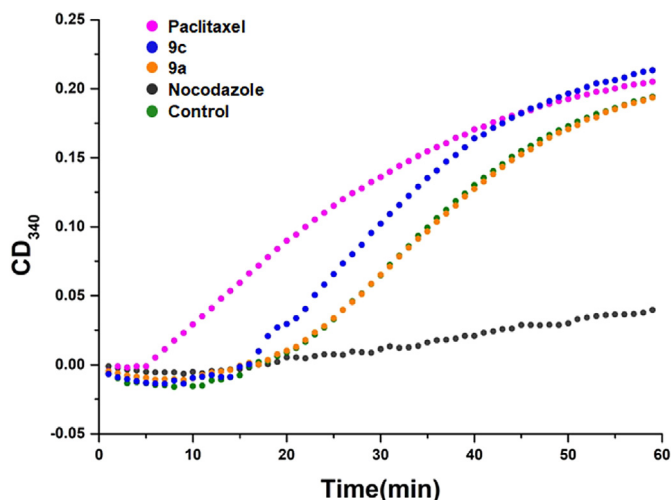


**Fig. 7.** Effects of compounds **9a** and **9c** on cell-free tubulin polymerization. The purified tubulin was incubated at 37 °C in a reaction buffer, and exposed to vehicle control or test compounds. Absorbance at 340 nm was monitored at 37 °C every 30 s for 60 min.

and **9c** showed comparable activity against C-RAF, with marginal preponderance for compound **9c** ( $IC_{50} = 0.229 \mu\text{M}$ ). Based on the aforementioned findings, C-RAF and its homologues B-RAF<sup>wild</sup>, B-RAF<sup>V600E</sup> stood as the main target kinases inhibited by these quinoline arylamide hybrids.

Furthermore, and to construct a reliable SAR for these new anilinoquinoline chemotypes, we examined the  $IC_{50}$  values of compounds **8b**, the 3,5-trifluoromethylphenyl derivative, and **9a–e** against B-RAF<sup>wild</sup>, B-RAF<sup>V600E</sup> and C-RAF kinases (Table 10). As revealed from the results, compounds **9a–e** exerted distinguishing inhibitory effects to **8b** for all tested RAF kinases. Such findings underscore the significance of existence of cyclic amine neighboring to 3-trifluoromethylphenyl for achieving good RAF inhibitory activity. Regarding **9a–e** series, all compounds showed 2–4 folds selectivity for C-RAF than B-RAF<sup>V600E</sup>. Moreover, they displayed modest to moderate activity towards B-RAF<sup>wild</sup>. The two piperazines derivatives **9a** and **9c** emerged as the most active members against all examined kinases, surpassing their corresponding morpholine analogs **9b** and **9d**, respectively. The ethylpiperazine derivative **9c** manifested the best activity with  $IC_{50}$  of

**Table 9**

*In vitro* biochemical activity ( $IC_{50}$ ,  $\mu\text{M}$ )<sup>a</sup> of compounds **9a** and **9c** against C-RAF, DDR1 and TrKA kinases.

Compound No.	$IC_{50}$ ( $\mu\text{M}$ ) <sup>a</sup>		
	C-RAF	DDR1	TrKA
<b>9a</b>	0.370	2.25	34.0
<b>9c</b>	0.229	0.538	1.67
Staurosporine	-	2.89	1.67
GW5074	0.00948	-	-

<sup>a</sup> Compounds were tested in a 10-dose singlicate  $IC_{50}$  mode with 3-fold serial dilution starting at 20  $\mu\text{M}$  (**9c**) or 100  $\mu\text{M}$  (**9a**), and the reactions were carried out at 10  $\mu\text{M}$  ATP.

**Table 10**

*In vitro* enzymatic activity ( $IC_{50}$ ,  $\mu\text{M}$ ) of compounds **8b** and **9a–e** over B-RAF<sup>WT</sup>, B-RAF<sup>V600E</sup> and C-RAF kinases.

Compound No.	$IC_{50}$ ( $\mu\text{M}$ ) <sup>a</sup>		
	B-RAF <sup>WT</sup>	B-RAF <sup>V600E</sup>	C-RAF
<b>8b</b>	>100	9.45	4.79
<b>9a</b>	2.94	1.46	0.370 <sup>b</sup>
<b>9b</b>	40.9	4.57	1.44
<b>9c</b>	2.23	0.888	0.229 <sup>b</sup>
<b>9d</b>	5.87	1.49	0.616
<b>9e</b>	9.28	1.10	0.414
GW5074	0.0126	0.00749	0.00736

<sup>a</sup> Compounds were tested in a 10-dose singlicate  $IC_{50}$  mode with 3-fold serial dilution starting at 20  $\mu\text{M}$  or 100  $\mu\text{M}$ , and the reactions were carried out at 10  $\mu\text{M}$  ATP.

<sup>b</sup> Data are taken from Table 9.

0.229  $\mu\text{M}$  and 0.888  $\mu\text{M}$  against C-RAF and B-RAF<sup>V600E</sup>, respectively. Compound **9a** comes second with  $IC_{50}$  of 0.370  $\mu\text{M}$  and 1.46  $\mu\text{M}$  against C-RAF and B-RAF<sup>V600E</sup>, respectively. Replacing the methylpiperazine moiety of **9a** with morpholine **9b** resulted in 3–4 folds drop in activity (C-RAF;  $IC_{50} = 1.44 \mu\text{M}$ , B-RAF<sup>V600E</sup>;  $IC_{50} = 4.57 \mu\text{M}$ ), similar to the case for compounds **9c** and **9d**. While comparing compounds **9d** and **9e**, it was found that appendage of 4-methylimidazole instead of morpholine is relatively favorable for attenuating the kinase activity of B-RAF<sup>V600E</sup> and C-RAF.

In agreement with the aforementioned cell-free assay findings, both compounds **9a** and **9c** exhibited high cellular potencies, with sub-micromolar  $GI_{50}$  values, towards the B-RAF<sup>V600E</sup> over-expressing cell lines such as colon cancer cells (COLO 205 and

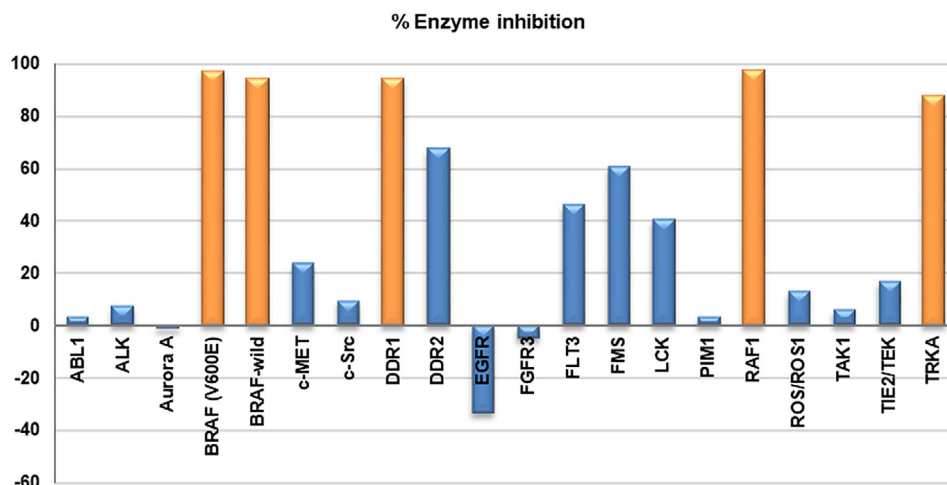


**Fig. 8.** Inhibition percentages of compound **9c** (10  $\mu\text{M}$  concentration) over a panel of 20 oncogenic kinases.

HT29), and melanoma cells (MALME-3M, SK-MEL-28, and SK-MEL-5). Moreover, C-RAF is commonly overexpressed in the absence of oncogenic mutations in 50% of renal-cell carcinoma (RCC) [53], as well as being associated with poor prognosis in ovarian cancer [54]. Accordingly, the remarkable anticancer effects of **9a** and **9c** over a number of RCC and ovarian cancer cell lines may stem from their C-RAF kinase inhibition. Considering both cell-based and cell-free assay results, it was obvious that both compound **9a** and **9c** are dual B-RAF<sup>V600E</sup>/C-RAF kinase inhibitors with potent anticancer activity over diverse cancer cell lines. However, they also possess pronounced anticancer activities against certain RAF independent cell lines, which may be attributed to the existence of other underlying mechanism(s), like apoptosis induction and microtubule stabilization, responsible for the antiproliferative activity of **9a** and **9c** towards those cell lines.

### 2.7. Molecular docking study

In order to rationalize the observed RAF kinase inhibitory results from a 3D structural perspective, compounds **8b** and **9a–e** were docked in the catalytic kinase domains of B-RAF<sup>V600E</sup> (PDB code: 1UWJ) [55] and C-RAF homology model. The molecular docking was performed by inserting the compounds into the sorafenib binding site of B-RAF<sup>V600E</sup> and C-RAF homology model. Compounds **9a–e** showed a highly similar binding mode with the both homologous kinases (Figs. 9–11). The ability of compounds **9a–e** to form two crucial hydrogen bonds with B-RAF<sup>V600E</sup> and C-RAF kinases mainly contribute to their affinities for well binding (Figs. S1 and S2, supplementary data). The critical hydrogen bonds for proper binding were formed between (1) hydrogen of amine

moiety in central amide bond and side chain carboxylate of catalytic Glu501 (B-RAF<sup>V600E</sup>)/Glu393 (C-RAF), (2) hydrogen of 5-methoxyquinoline moiety and the carbonyl oxygen of Cys532 (B-RAF<sup>V600E</sup>)/Cys424 (C-RAF) in the hinge region. The  $\pi$ -alkyl interactions between the methoxy moiety and the surrounding hydrophobic residues were consistent across all compounds. In particular, the methoxy carbon occupies the ATP adenine binding site, interacting with two aromatic residues, which are Trp531 (B-RAF<sup>V600E</sup>)/Trp423 (C-RAF) of the hinge region and Phe583 (B-RAF<sup>V600E</sup>)/Phe475 (C-RAF) at the end of the catalytic loop [55]. In addition, the quinoline ring showed  $\pi$ -alkyl interaction with side chain alkyl group of Val471 (B-RAF<sup>V600E</sup>)/Val363 (C-RAF) in the P-loop region. Both phenyl and pyridine groups of quinoline ring were involved in  $\pi$ -alkyl interactions with the side chain alkyl groups of Ile463 (B-RAF<sup>V600E</sup>)/Ile355 (C-RAF) and Ala481 (B-RAF<sup>V600E</sup>)/Ala373 (C-RAF) residues in the P-loop region, respectively. Also, the aliphatic side chain of Lys483 (B-RAF<sup>V600E</sup>)/Lys375 (C-RAF) shared  $\pi$ -alkyl interactions with central phenyl ring of the inhibitors. Finally, trifluoromethyl phenyl ring was engaged in  $\pi$ -alkyl interactions with side chain alkyl group of Leu567 (B-RAF<sup>V600E</sup>)/Leu459 (C-RAF).

In this study, we designed certain kinase inhibitor candidates based on replacing one trifluoromethyl group of compound **8b** with bulky cyclic amine groups, such as piperazine (**9a** and **9c**), morpholine (**9b** and **9d**), and imidazole (**9e**). It was confirmed through our docking study that the compound's efficacy and binding mode vary according to the cyclic amine group. The bulky heterocyclic group was stabilized by interacting with Asp594 (B-RAF<sup>V600E</sup>)/Asp486 (C-RAF) in DFG loop. Two hydrogens of the piperazine and morpholine were engaged in hydrogen bonding with the side chain

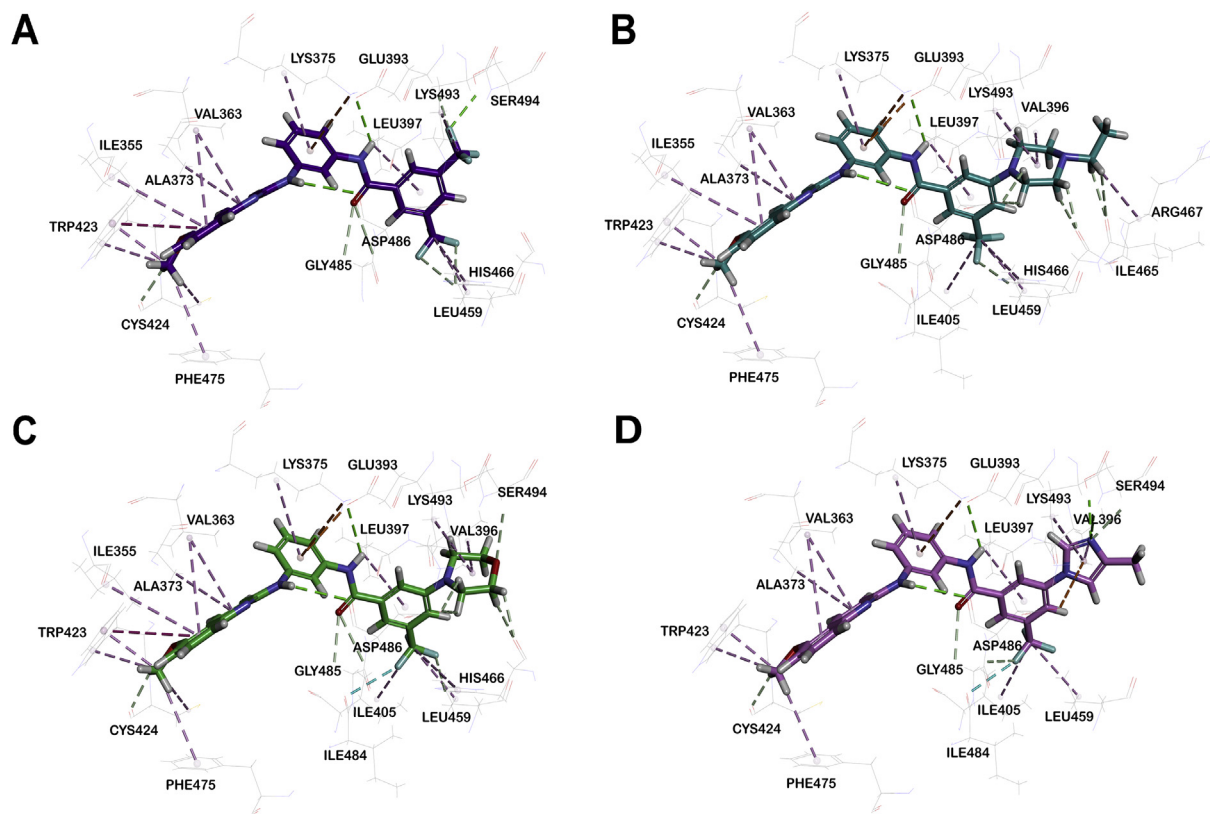


**Fig. 9.** The putative binding mode of compounds **8b** (A), **9c** (B), **9d** (C), and **9e** (D) in the catalytic kinase domain of C-RAF homology model. For clarity purpose, only residues having interactions were shown. Compounds **8b**, **9c**, **9d**, and **9e** are shown in stick model and surrounding residues were shown in line model, and various interactions are shown in dashes.

carboxylates of aspartic acid in both B-RAF<sup>V600E</sup> and C-RAF homology models. *N*-substituted piperazine (**9a** and **9c**) showed alkyl interactions with three hydrophobic residues; Val504 (B-RAF<sup>V600E</sup>)/Val396 (C-RAF), Lys601 (B-RAF<sup>V600E</sup>)/Lys493 (C-RAF), and Ile573 (B-RAF<sup>V600E</sup>)/Ile465 (C-RAF). However, their corresponding morpholine derivatives (**9b** and **9d**) shared interactions with only Val396 and Lys493 in C-RAF. In B-RAF<sup>V600E</sup>, **9d** displayed hydrophobic interactions with Val504 and Lys601, but in **9b** such alkyl interactions with hydrophobic residues Val504 and Lys601 were lacked. Such findings may emphasize the hypothesis that the increased hydrophobicity and bulkiness of *N*-substituted piperazines over morpholine might be advantageous to enhance the hydrophobic interactions with the target proteins. Regarding compound **9e**, the two RAF models had different binding modes. One was the  $\pi$ -anion interaction between the imidazole ring and the side chain carboxylate of Asp486 (C-RAF), and the other was the hydrogen bond between the hydrogen of the imidazole ring and the side chain carboxylate of Asp594 (B-RAF<sup>V600E</sup>) (Figs. S1 and S2, supplementary data). In the case of compound **8b** (Fig. 9), there was a halogen interaction between the side chain carboxylate of Asp594 (B-RAF<sup>V600E</sup>) and fluorine of trifluoromethyl moiety, but such interaction was lacked in C-RAF. However, a hydrogen bond was formed between the carbonyl oxygen of Asp486 (C-RAF) and the hydrogen of the amine tethering the central phenyl group with the quinoline moiety. In addition, the interactions of **8b** with catalytic loop (Ile572–Asn580 in B-RAF<sup>V600E</sup>/Ile464–Asn472 in C-RAF) were weaker than other inhibitors due to the shorter trifluoromethyl moiety compared with other bulky heterocyclic groups, which consequently destabilize the active conformation than other inhibitors. This observation is consistent with the lowest RAF kinase inhibitory effect of **8b**.

When the ethylpiperazine was introduced at *meta* position, close to 3-trifluoromethyl (**9c**), the RAF kinase inhibitory effect was superior to that of *para* position (**9a**) (Fig. 10). In the case of *meta* position (**9c**), the trifluoromethyl moiety shared alkyl interactions with B-RAF<sup>V600E</sup> Ile513 and Ile592, and the bulky piperazine ring interacted with B-RAF<sup>V600E</sup> residues Val504 and Lys601 through alkyl interactions, however in *para* position (**9a**), such interaction was not observed. Therefore, compound **9c** could interact more strongly with the RAF protein than **9a**, so that lipophilic trifluoromethyl phenyl ring would be inserted into a hydrophobic pocket form between the  $\alpha$ C and  $\alpha$ E helices and DFG motif and catalytic loop (Fig. 10). This tendency is consistently observed in compounds **9b** (*para*) and **9d** (*meta*) where morpholine was substituted (Fig. 11).

In the case of **9c**, the carbon of ethyl piperazine displayed an alkyl interaction with the side chain alkyl group of Arg574 (B-RAF<sup>V600E</sup>)/Arg467 (C-RAF) that is located in the highly conserved HRD (His–Arg–Asp) motif of the C lobe catalytic loop. In the case of the oncogenic B-RAF<sup>V600E</sup> mutant, the negative charge of the Glu600 residue could form a salt bridge interaction with the Lys507 and/or Arg575 residue, stabilizing the active conformation to mimic the Thr599 and Ser602 phosphorylation effects [56]. As shown in the results of this study, the loss of positive charge due to the interaction between Arg575 and **9c** weakens the binding with the existing Glu600, thereby preventing the activation loop from adopting the active structure to facilitate ATP binding (Figs. 9B and 10B). Therefore, such finding strongly emphasizes the experimental results that **9c**, which only interacts with Arg575, best inhibits the RAF kinase activity.

Concerning compound **9d**, where the morpholine is substituted at the *meta* position, trifluoromethyl fluorine and backbone amide bond carboxylate in Ile592 (B-RAF<sup>V600E</sup>)/Ile484 (C-RAF) showed a halogen interaction, so that the binding is more stable than **9b** that lacked such interaction (Fig. 11). Finally, two additional interactions

between C-RAF and inhibitor candidates were observed. One is the hydrogen bond between the hydrogen of the amine linking the central phenyl group with the quinoline moiety and the carbonyl oxygen of Asp486, and the other was the  $\pi$ -anion interaction between the side chain carbonyl oxygen of Glu393 and central phenyl ring. However, such additional binding was not seen in B-RAF. The results of this docking study are consistent with the overall observed activity of the inhibitor candidates in C-RAF compared to B-RAF.

### 3. Conclusion

In this study, a new series of 2-anilinoquinoline based arylamides, featuring diverse substituents on the terminal aryl ring along with different amide attachment positions, has been designed and synthesized as potential anticancer agents. A selected array of target molecules was evaluated for its antiproliferative activity over a panel of 60 cancer cell lines at 10  $\mu$ M concentration at NCI. Our SAR study pointed out that attachment of amide to the *meta*-position of 2-anilinoquinoline scaffold is favorable for anticancer activity. In addition, 3-trifluoromethylphenyl group substituted with cyclic amines and possessing increased steric characters was found to be optimal for anticancer activity. Among the examined compounds, piperazines derivatives **9a** and **9c** have elicited remarkable broad spectrum anticancer activities and were further tested at five-dose testing mode in comparison with imatinib. Both compounds **9a** and **9c** exerted superior anticancer potencies to imatinib over most of the tested cell lines, including MDR cells, with sub-micromolar or low one-digit micromolar GI<sub>50</sub> values. A detailed mechanistic study for the anticancer activity of **9a** and **9c** in HCT-116 colon cancer cell line revealed their ability to trigger significant apoptotic events and morphological alternations in cancer cells. Furthermore, both **9a** and **9c** induced cell cycle arrest at G0/G1 phase, and exerted a dose-dependent increase in the early apoptotic populations. Moreover, the ethylpiperazine **9c** showed microtubule polymerization stabilizing effect comparable to paclitaxel. Kinase profiling of **9c** showed its highly inhibitory effects towards B-RAF<sup>wild</sup>, B-RAF<sup>V600E</sup> and C-RAF kinases. Further biochemical evaluations of **8b** and **9a–e** revealed that compounds **9a** and **9c** have the best activity over RAF kinases, and the obtained kinase results were justified by molecular docking. In view of the presented data, compounds **9a** and **9c** might serve as promising candidates for development of new potent and efficacious anticancer chemotherapeutics.

### 4. Experimental

#### 4.1. General

All reactions and manipulations were conducted utilizing standard Schlenk techniques. All solvents and reagents were obtained from commercial suppliers and were used without further purification. The reaction progress was monitored on TLC plate (Merck, silica gel 60 F<sub>254</sub>). Flash column chromatography was carried out using silica gel (Merck, 230–400 mesh) and the mobile phase solvents are indicated as a mixed solvent with either given volume-to-volume ratios or as a percentage. <sup>1</sup>H and <sup>13</sup>C NMR spectra were recorded on a Bruker Avance 300 or 400 MHz spectrometer, using appropriate deuterated solvents, as noted. Chemical shifts ( $\delta$ ) are given in parts per million (ppm) upfield from tetramethylsilane (TMS) as internal standard, and s, d, t, and m are designated as singlet, doublet, triplet and multiplet, respectively. Coupling constants (*J*) are reported in hertz (Hz). High resolution mass spectra (HRMS) were recorded on JMS 700 (Jeol, Japan) mass spectrometer, with magnetic sector–electric sector double focusing

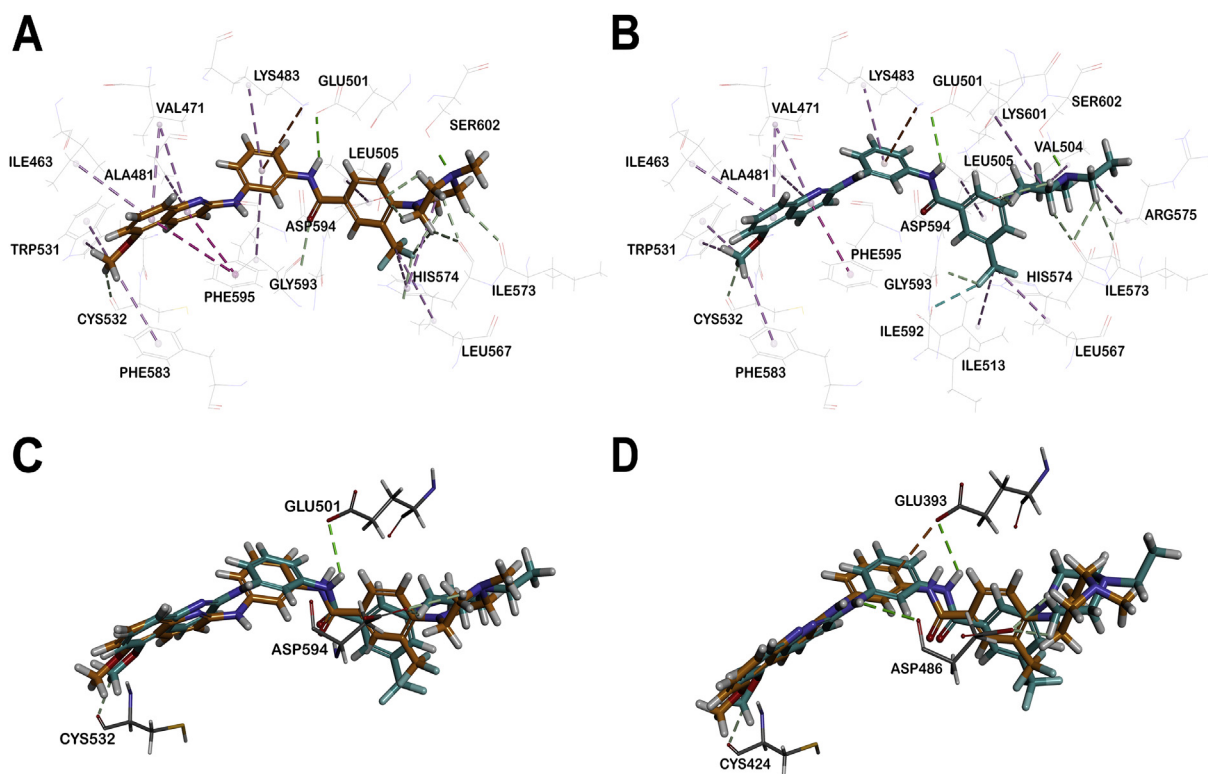


**Fig. 10.** The binding mode of compound **9a** (A) and **9c** (B) in the catalytic kinase domain of B-RAF<sup>V600E</sup> model. For clarity purpose, only residues having interactions were shown. Compounds **9a** and **9c** are shown in stick model and surrounding residues were shown in line model, and various interactions are shown in dashes. 3D structural overlay of compounds **9a** (orange) and **9c** (skyblue) in the catalytic kinase domain of B-RAF<sup>V600E</sup> (C) and C-RAF (D) homology model. The key important three hydrogen bonds are shown in green. (For interpretation of the references to color in this figure legend, the reader is referred to the Web version of this article.)

mass analyzer, and FAB+ ion mode. The purity of all final compounds was >95%, as determined by <sup>1</sup>H NMR. Compounds **1–4** were prepared adopting the reported procedure [12].

#### 4.2. General procedure for synthesis of compounds **5a** and **5b**

A mixture of compound **4** (0.2 g, 1.03 mmol) and *p(m)*-nitroaniline (0.14 g, 1.03 mmol) were fused at 160 °C for 2 h. The reaction mixture was cooled, dissolved in DCM and concentrated under reduced pressure to afford the desired product, which was purified by crystallization from ethanol.

##### 4.2.1. 5-Methoxy-*N*-(4-nitrophenyl)quinolin-2-amine (**5a**)

Yellow solid; yield 98%; <sup>1</sup>H NMR (400 MHz, DMSO-*d*<sub>6</sub>) δ 10.82 (br. s, 1H), 8.39 (d, *J* = 9.2 Hz, 1H), 8.23 (d, *J* = 9.2 Hz, 2H), 8.16 (d, *J* = 9.2 Hz, 2H), 7.60 (t, *J* = 8.4 Hz, 1H), 7.40 (d, *J* = 8.4 Hz, 1H), 7.18 (d, *J* = 9.2 Hz, 1H), 6.91 (d, *J* = 8.0 Hz, 1H), 3.94 (s, 3H); <sup>13</sup>C NMR (100 MHz, DMSO-*d*<sub>6</sub>) δ 155.19, 153.30, 147.31, 146.16, 140.78, 133.03, 130.94, 125.43, 118.37, 118.27, 115.44, 113.36, 103.84, 56.05.

##### 4.2.2. 5-Methoxy-*N*-(3-nitrophenyl)quinolin-2-amine (**5b**)

Yellow solid; yield 96%; <sup>1</sup>H NMR (400 MHz, DMSO-*d*<sub>6</sub>) δ 10.82 (br. s, 1H), 8.87 (s, 1H), 8.43 (d, *J* = 9.3 Hz, 1H), 8.08 (dd, *J* = 8.0, 1.6 Hz, 1H), 7.97 (dd, *J* = 8.0, 1.6 Hz, 1H), 7.70–7.61 (m, 2H), 7.37 (d, *J* = 8.4 Hz, 1H), 7.18 (d, *J* = 9.3 Hz, 1H), 6.95 (d, *J* = 8.0 Hz, 1H), 3.95 (s, 3H); <sup>13</sup>C NMR (100 MHz, DMSO-*d*<sub>6</sub>) δ 155.43, 153.20, 148.59, 143.05, 140.27, 134.78, 132.08, 130.77, 127.38, 118.38, 115.49, 115.29, 114.51, 112.97, 104.47, 56.23.

#### 4.3. General procedure for synthesis of compounds **6a** and **6b**

Stannous chloride dihydrate (11.2 g, 51.65 mmol) was added to a solution of compound **5a** or **5b** (3.05 g, 10.33 mmol) in absolute ethanol (150 mL), and the reaction mixture was heated under reflux for 1 h. Sodium borohydride (0.18 g, 5.17 mmol) was added portionwise to the reaction mixture and the mixture was allowed to reflux for additional 0.5 h. The reaction mixture was cooled, the solvent was evaporated under reduced pressure, and the concentrate was dissolved in water. The resultant solution was rendered alkaline with 40% aq. NaOH and was extracted with ethyl acetate (3 × 200 mL). The organic layers were collected, washed with water, brine solution, and dried over anhydrous Na<sub>2</sub>SO<sub>4</sub>. The solvent was evaporated under reduced pressure to give yellow residue, which was purified by column chromatography using 1% MeOH in DCM to afford the titled compound as pure yellow solid.

##### 4.3.1. *N*<sup>1</sup>-(5-Methoxyquinolin-2-yl)benzene-1,4-diamine (**6a**)

Yield 92%; <sup>1</sup>H NMR (400 MHz, CDCl<sub>3</sub>) δ 8.25 (d, *J* = 9.2 Hz, 1H), 7.45 (t, *J* = 8.4 Hz, 1H), 7.30 (d, *J* = 8.4 Hz, 1H), 7.23–7.19 (m, 2H), 6.80 (d, *J* = 9.2 Hz, 1H), 6.71–6.68 (m, 2H), 6.61 (d, *J* = 7.8 Hz, 1H), 3.94 (s, 3H), 3.73 (br. s, 2H); <sup>13</sup>C NMR (100 MHz, CDCl<sub>3</sub>) δ 156.32, 155.57, 148.40, 143.63, 132.62, 130.72, 129.91, 125.07, 118.45, 115.89, 115.46, 109.18, 101.55, 55.59.

##### 4.3.2. *N*<sup>1</sup>-(5-Methoxyquinolin-2-yl)benzene-1,3-diamine (**6b**)

Yield 95%; <sup>1</sup>H NMR (300 MHz, CDCl<sub>3</sub>) δ 8.30 (d, *J* = 9.1 Hz, 1H), 7.47 (t, *J* = 7.8 Hz, 1H), 7.36 (d, *J* = 8.5 Hz, 1H), 7.10 (t, *J* = 8.0 Hz, 1H), 6.97–6.94 (m, *J* = 2H), 6.88 (br. s, 1H), 6.80 (dd, *J* = 6.8, 1.1 Hz, 1H), 6.64 (d, *J* = 7.7 Hz, 1H), 6.40 (dt, *J* = 7.9, 0.7 Hz, 1H), 3.94 (s, 3H), 3.70 (br. s, 2H); <sup>13</sup>C NMR (75 MHz, CDCl<sub>3</sub>) δ 155.50, 154.90, 148.76, 147.48,

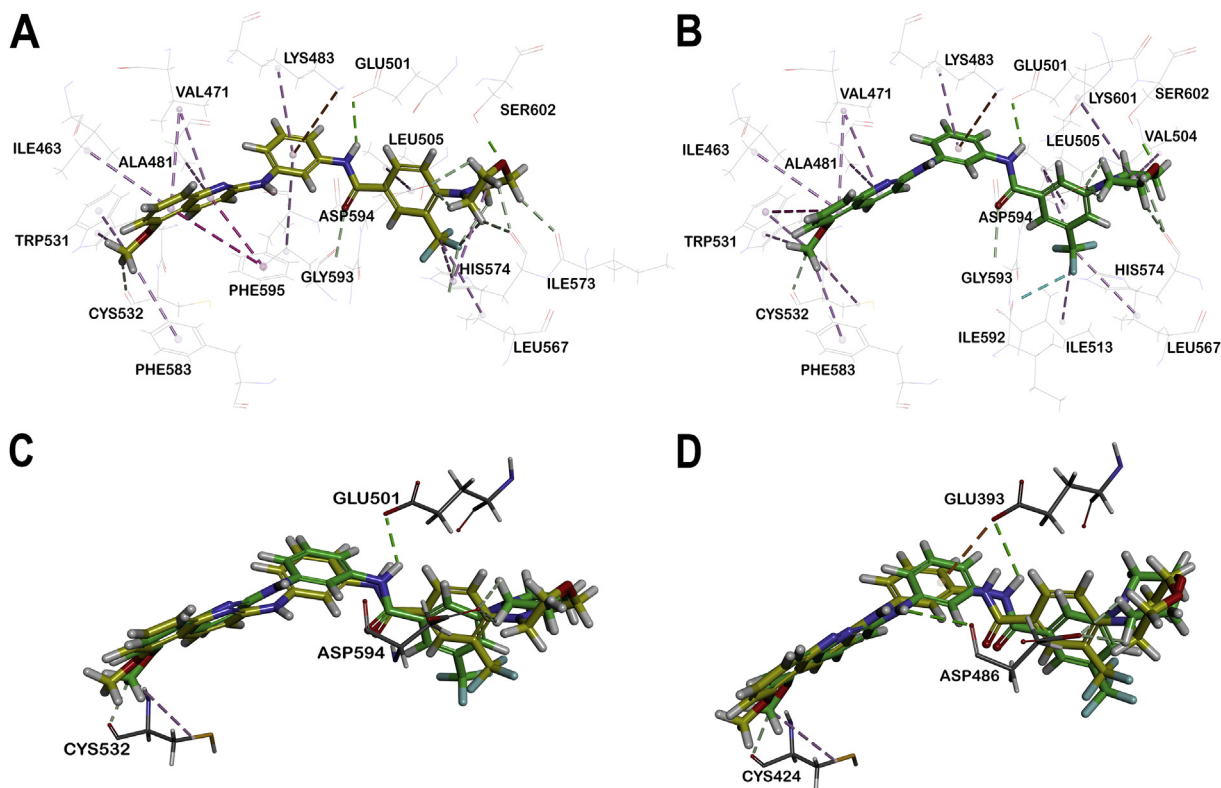


**Fig. 11.** The putative binding mode of compounds **9b** (A) and **9d** (B) in the catalytic kinase domain of B-RAF<sup>V600E</sup> model. For clarity purpose, only residues having interactions were shown. **9b** and **9d** are shown in stick model and the surrounding residues were shown in line model. Various interactions are shown in dashes. 3D structural overlay of compounds **9b** (yellow) and **9d** (green) in the catalytic kinase domain of B-RAF<sup>V600E</sup> (C) and C-RAF (D) homology model. The key important three hydrogen bonds are shown in green. (For interpretation of the references to color in this figure legend, the reader is referred to the Web version of this article.)

141.25, 132.41, 130.03, 129.79, 119.20, 115.90, 110.92, 110.46, 110.15, 107.23, 101.87, 55.62.

56.09; HRMS (FAB<sup>+</sup>) *m/z* calcd for C<sub>24</sub>H<sub>18</sub>ClF<sub>3</sub>N<sub>3</sub>O<sub>2</sub> [M+H]<sup>+</sup>: 472.1039, found: 472.1036.

#### 4.4. General procedure for synthesis of compounds **7a–e**, **8a–e** and **9a–e**

*N,N*-Diisopropylethylamine (DIPEA) (0.128 mL, 0.72 mmol) and HATU (0.168 g, 0.442 mmol) were added to a mixture of compound **6a** or **6b** (0.045 g, 0.17 mmol) and the appropriate aryl/heteroaryl carboxylic acid (0.34 mmol) in anhydrous DMF (2 mL) under argon atmosphere. The reaction mixture was stirred at rt for 18 h or at 70–80 °C for 2.5–18 h (for **7e**, **8e**, **9c** and **9e**), and then quenched with water (30 mL). The aqueous layer was extracted with ethyl acetate (3 × 15 mL), and the combined organic layers was washed with water and brine, dried over anhydrous Na<sub>2</sub>SO<sub>4</sub>, and filtered. The solvent was evaporated under reduced pressure, and the resultant residue was purified by column chromatography using the appropriate elution system to afford the target compounds in their pure form.

##### 4.4.1. 4-Chloro-*N*-(4-((5-methoxyquinolin-2-yl)amino)phenyl)-3-(trifluoromethyl)benzamide (**7a**)

Column chromatography was performed using 10% ethyl acetate in DCM. White solid; yield 48.7%; <sup>1</sup>H NMR (400 MHz, DMSO-*d*<sub>6</sub>) δ 10.47 (br. s, 1H), 9.44 (br. s, 1H), 8.42 (s, 1H), 8.30–8.23 (m, 2H), 8.00–7.92 (m, 3H), 7.73–7.71 (m, 2H), 7.50 (t, *J* = 8.0 Hz, 1H), 7.30 (d, *J* = 8.3 Hz, 1H), 7.03 (dd, *J* = 9.1, 1.7 Hz, 1H), 6.77 (d, *J* = 7.8 Hz, 1H), 3.94 (s, 3H); <sup>13</sup>C NMR (100 MHz, DMSO-*d*<sub>6</sub>) δ 163.11, 155.43, 154.84, 148.44, 138.34, 134.82, 134.14, 133.74, 132.55, 132.36, 131.41, 130.04, 127.47, 127.41, 121.81, 121.69, 119.40, 119.03, 115.05, 113.21, 102.60,

##### 4.4.2. *N*-(4-((5-Methoxyquinolin-2-yl)amino)phenyl)-3,5-bis(trifluoromethyl)benzamide (**7b**)

Column chromatography was performed using 5% ethyl acetate in DCM. White solid; yield 53.6%; <sup>1</sup>H NMR (400 MHz, DMSO-*d*<sub>6</sub>) δ 10.62 (s, 1H), 9.46 (s, 1H), 8.64 (s, 2H), 8.37 (s, 1H), 8.25 (d, *J* = 9.1 Hz, 1H), 8.01 (d, *J* = 9.0 Hz, 2H), 7.74 (d, *J* = 9.0 Hz, 2H), 7.50 (t, *J* = 8.1 Hz, 1H), 7.31 (d, *J* = 8.4 Hz, 1H), 7.03 (d, *J* = 9.1 Hz, 1H), 6.80 (d, *J* = 7.8 Hz, 1H), 3.95 (s, 3H); <sup>13</sup>C NMR (100 MHz, DMSO-*d*<sub>6</sub>) δ 162.47, 155.43, 154.83, 148.42, 138.52, 137.77, 132.33, 131.43, 131.10, 130.77, 130.04, 128.90, 124.99, 122.28, 121.80, 119.41, 119.02, 115.07, 113.22, 102.61, 56.09; HRMS (FAB<sup>+</sup>) *m/z* calcd for C<sub>25</sub>H<sub>18</sub>F<sub>6</sub>N<sub>3</sub>O<sub>2</sub> [M+H]<sup>+</sup>: 506.1303, found: 506.1301.

##### 4.4.3. 6-Chloro-*N*-(4-((5-methoxyquinolin-2-yl)amino)phenyl)picolinamide (**7c**)

Column chromatography was performed using a mixture of hexane–ethyl acetate (2:1, v/v). White solid; yield 36%; <sup>1</sup>H NMR (400 MHz, CDCl<sub>3</sub>) δ 9.70 (br. s, 1H), 8.37 (d, *J* = 9.1 Hz, 1H), 8.27 (d, *J* = 7.6 Hz, 1H), 7.90 (t, *J* = 7.8 Hz, 1H), 7.80 (d, *J* = 8.8 Hz, 2H), 7.65 (d, *J* = 8.8 Hz, 2H), 7.53 (t, *J* = 8.2 Hz, 2H), 7.41 (d, 8.4Hz, 1H), 6.95 (d, *J* = 9.1 Hz, 1H), 6.84 (br. s, 1H), 6.70 (d, *J* = 7.7 Hz, 1H), 4.00 (s, 3H); <sup>13</sup>C NMR (100 MHz, CDCl<sub>3</sub>) δ 160.29, 155.47, 154.53, 150.55, 150.01, 148.67, 140.27, 136.98, 132.49, 129.81, 127.17, 121.10, 121.00, 120.95, 120.86, 119.30, 115.90, 110.33, 101.93, 55.60; HRMS (FAB<sup>+</sup>) *m/z* calcd for C<sub>22</sub>H<sub>18</sub>ClN<sub>4</sub>O<sub>2</sub> [M+H]<sup>+</sup>: 405.1118, found: 405.1115.

#### 4.4.4. *N*-(4-((5-Methoxyquinolin-2-yl)amino)phenyl)quinoline-6-carboxamide (**7d**)

Column chromatography was performed using 2% MeOH in DCM. White solid; yield 73%; <sup>1</sup>H NMR (400 MHz, MeOD) δ 8.94 (dd, *J* = 4.3, 1.7 Hz, 1H), 8.54 (d, *J* = 1.9 Hz, 1H), 8.47 (dd, *J* = 8.6, 0.9 Hz, 1H), 8.28 (dd, *J* = 9.6, 4.0 Hz, 2H), 8.13 (d, *J* = 8.8 Hz, 1H), 7.85 (d, *J* = 9.0 Hz, 2H), 7.72 (d, *J* = 9.0 Hz, 2H), 7.61 (q, *J* = 4.4 Hz, 1H), 7.47 (t, *J* = 8.0 Hz, 1H), 7.30 (d, *J* = 8.4 Hz, 1H), 6.91 (d, *J* = 9.1 Hz, 1H), 6.75 (d, *J* = 7.4 Hz, 1H), 3.97 (s, 3H); <sup>13</sup>C NMR (100 MHz, MeOD) δ 166.22, 155.60, 154.85, 151.66, 148.57, 138.00, 137.75, 133.31, 132.76, 132.02, 131.67, 129.62, 128.33, 128.08, 127.78, 122.09, 121.60, 119.75, 117.91, 115.21, 111.62, 101.90, 54.84; HRMS (FAB+) *m/z* calcd for C<sub>26</sub>H<sub>21</sub>N<sub>4</sub>O<sub>2</sub> [M+H]<sup>+</sup>: 421.1664, found: 421.1663.

#### 4.4.5. *N*-(4-((5-Methoxyquinolin-2-yl)amino)phenyl)-2,3-dihydrobenzo[*b*] [1,4]dioxine-6-carboxamide (**7e**)

Column chromatography was performed using a mixture of hexane-ethyl acetate (1:1, v/v). White solid; yield 62.7%; <sup>1</sup>H NMR (300 MHz, DMSO-*d*<sub>6</sub>) δ 9.98 (br. s, 1H), 9.37 (br. s, 1H), 8.22 (d, *J* = 8.9 Hz, 1H), 7.92 (d, *J* = 8.3 Hz, 2H), 7.71 (d, *J* = 8.3 Hz, 2H), 7.54–7.45 (m, 3H), 7.28 (d, *J* = 8.2 Hz, 1H), 6.99 (d, *J* = 8.0 Hz, 2H), 6.77 (d, *J* = 7.5 Hz, 1H), 4.31 (s, 4H), 3.93 (s, 3H); <sup>13</sup>C NMR (75 MHz, DMSO-*d*<sub>6</sub>) δ 164.58, 155.43, 154.89, 148.48, 146.67, 143.40, 137.71, 133.30, 131.36, 130.01, 128.43, 121.57, 121.44, 119.36, 117.27, 117.06, 115.00, 113.17, 102.53, 64.86, 64.50, 56.08; HRMS (FAB+) *m/z* calcd for C<sub>25</sub>H<sub>22</sub>N<sub>3</sub>O<sub>4</sub> [M+H]<sup>+</sup>: 428.1610, found: 428.1613.

#### 4.4.6. 4-Chloro-*N*-(3-((5-methoxyquinolin-2-yl)amino)phenyl)-3-(trifluoromethyl)benzamide (**8a**)

Column chromatography was performed using 5% ethyl acetate in DCM. White solid; yield 59.6%; <sup>1</sup>H NMR (400 MHz, DMSO-*d*<sub>6</sub>) δ 10.53 (br. s, 1H), 9.50 (br. s, 1H), 8.52 (s, 1H), 8.42 (d, *J* = 2.0 Hz, 1H), 8.30 (dd, *J* = 8.4, 2.0 Hz, 1H), 8.25 (d, *J* = 9.0 Hz, 1H), 7.95 (d, *J* = 8.4 Hz, 1H), 7.80 (m, 1H), 7.51 (t, *J* = 8.1 Hz, 1H), 7.36–7.31 (m, 3H), 7.07 (d, *J* = 9.1 Hz, 1H), 6.80 (d, *J* = 7.4 Hz, 1H), 3.95 (s, 3H); <sup>13</sup>C NMR (100 MHz, DMSO-*d*<sub>6</sub>) δ 163.64, 155.40, 154.87, 148.37, 142.19, 139.34, 134.92, 133.93, 132.37, 131.45, 130.02, 129.15, 127.57, 126.94, 119.54, 115.10, 114.92, 114.04, 113.30, 111.32, 102.70, 56.11; HRMS (FAB+) *m/z* calcd for C<sub>24</sub>H<sub>18</sub>ClF<sub>3</sub>N<sub>3</sub>O<sub>2</sub> [M+H]<sup>+</sup>: 472.1039, found: 472.1036.

#### 4.4.7. *N*-(3-((5-Methoxyquinolin-2-yl)amino)phenyl)-3,5-bis(trifluoromethyl)benzamide (**8b**)

Column chromatography was performed using 5% ethyl acetate in DCM. Yellowish white solid; yield 70%; <sup>1</sup>H NMR (400 MHz, DMSO-*d*<sub>6</sub>) δ 10.67 (br. s, 1H), 9.52 (br. s, 1H), 8.64 (s, 2H), 8.54 (d, *J* = 1.9 Hz, 1H), 8.39 (s, 1H), 7.83 (dt, *J* = 7.3, 1.7 Hz, 1H), 7.52 (t, *J* = 8.1 Hz, 1H), 7.37–7.31 (m, 3H), 7.07 (d, *J* = 9.1 Hz, 1H), 6.81 (d, *J* = 7.4 Hz, 1H), 3.95 (s, 3H); <sup>13</sup>C NMR (100 MHz, DMSO-*d*<sub>6</sub>) δ 163.04, 155.41, 154.87, 148.36, 142.23, 139.17, 137.90, 131.46, 130.75, 130.03, 129.18, 129.06, 125.47, 124.99, 122.28, 119.53, 115.12, 114.15, 113.31, 111.43, 102.72, 56.11; HRMS (FAB+) *m/z* calcd for C<sub>25</sub>H<sub>18</sub>F<sub>6</sub>N<sub>3</sub>O<sub>2</sub> [M+H]<sup>+</sup>: 506.1303, found: 506.1306.

#### 4.4.8. 6-Chloro-*N*-(3-((5-methoxyquinolin-2-yl)amino)phenyl)picolinamide (**8c**)

Column chromatography was performed using a mixture of hexane-ethyl acetate (1:1, v/v). Yellow solid; yield 24.6%; <sup>1</sup>H NMR (300 MHz, CDCl<sub>3</sub>) δ 9.70 (s, 1H), 8.34 (d, *J* = 9.1 Hz, 1H), 8.22 (d, *J* = 7.6 Hz, 1H), 8.16 (d, *J* = 1.9 Hz, 1H), 7.84 (t, *J* = 7.8 Hz, 1H), 7.53–7.34 (m, 6H), 6.99 (br. s, 1H), 6.95 (d, *J* = 9.1 Hz, 1H), 6.66 (d, *J* = 7.4 Hz, 1H), 3.95 (s, 3H); <sup>13</sup>C NMR (75 MHz, CDCl<sub>3</sub>) δ 160.63, 155.46, 154.36, 150.45, 150.03, 148.61, 141.23, 140.28, 138.11, 132.50, 129.80, 129.76, 127.29, 121.20, 119.46, 116.13, 116.00, 114.14, 111.24, 110.86, 102.07, 55.61; HRMS (FAB+) *m/z* calcd for C<sub>22</sub>H<sub>18</sub>ClN<sub>4</sub>O<sub>2</sub>

[M+H]<sup>+</sup>: 405.1118, found: 405.1117.

#### 4.4.9. *N*-(3-((5-Methoxyquinolin-2-yl)amino)phenyl)quinoline-6-carboxamide (**8d**)

Column chromatography was performed using 35–50% ethyl acetate in DCM. Yellowish white solid; yield 79.6%; <sup>1</sup>H NMR (300 MHz, DMSO-*d*<sub>6</sub>) δ 10.50 (br. s, 1H), 9.49 (br. s, 1H), 9.02 (dd, *J* = 4.1, 1.6 Hz, 1H), 8.66 (s, 1H), 8.56 (d, *J* = 6.6 Hz, 2H), 8.30–8.23 (m, 2H), 8.16 (d, *J* = 8.8 Hz, 1H), 7.82 (d, *J* = 7.4 Hz, 1H), 7.65 (q, *J* = 4.2 Hz, 1H), 7.49 (t, *J* = 8.2 Hz, 1H), 7.36–7.31 (m, 3H), 7.07 (d, *J* = 9.1 Hz, 1H), 6.79 (d, *J* = 7.9 Hz, 1H), 3.93 (s, 3H); <sup>13</sup>C NMR (75 MHz, DMSO-*d*<sub>6</sub>) δ 165.63, 155.40, 154.92, 152.66, 149.22, 148.41, 142.17, 139.81, 137.64, 133.55, 131.41, 129.98, 129.54, 129.12, 128.88, 128.66, 127.56, 122.71, 119.58, 115.09, 113.94, 113.31, 111.20, 102.68, 56.11; HRMS (FAB+) *m/z* calcd for C<sub>26</sub>H<sub>21</sub>N<sub>4</sub>O<sub>2</sub> [M+H]<sup>+</sup>: 421.1664, found: 421.1663.

#### 4.4.10. *N*-(3-((5-Methoxyquinolin-2-yl)amino)phenyl)-2,3-dihydrobenzo[*b*] [1,4]dioxine-6-carboxamide (**8e**)

Column chromatography was performed using a mixture of hexane-ethyl acetate (1:1, v/v). White solid; yield 70.4%; <sup>1</sup>H NMR (400 MHz, CDCl<sub>3</sub>) δ 8.27 (d, *J* = 9.1 Hz, 1H), 8.20 (s, 1H), 7.93 (d, *J* = 1.9 Hz, 1H), 7.48–7.39 (m, 4H), 7.35 (dd, *J* = 8.4, 2.2 Hz, 1H), 7.30–7.23 (m, 2H), 7.19 (br. s, 1H), 6.89–6.84 (m, 2H), 4.24–4.20 (m, 4H), 3.93 (s, 3H); <sup>13</sup>C NMR (100 MHz, CDCl<sub>3</sub>) δ 165.40, 155.42, 154.49, 148.49, 146.68, 143.39, 141.04, 138.83, 132.29, 129.66, 129.51, 128.17, 120.65, 119.27, 117.27, 116.78, 115.93, 115.87, 114.63, 111.89, 111.10, 101.95, 64.51, 64.13, 55.56; HRMS (FAB+) *m/z* calcd for C<sub>25</sub>H<sub>22</sub>N<sub>3</sub>O<sub>4</sub> [M+H]<sup>+</sup>: 428.1610, found: 428.1607.

#### 4.4.11. *N*-(3-((5-Methoxyquinolin-2-yl)amino)phenyl)-4-(4-methylpiperazin-1-yl)-3-(trifluoromethyl)benzamide (**9a**)

Column chromatography was performed using 5–10% MeOH in DCM. White solid; yield 78.3%; <sup>1</sup>H NMR (400 MHz, Acetone-*d*<sub>6</sub>) δ 9.74 (s, 1H), 8.65 (br, 2H), 8.29 (t, *J* = 4.4 Hz, 2H), 8.25 (d, *J* = 8.0 Hz, 1H), 7.86 (d, *J* = 8.0 Hz, 1H), 7.55 (d, *J* = 8.4 Hz, 1H), 7.51–7.40 (m, 3H), 7.32 (t, *J* = 8.4 Hz, 1H), 7.07 (d, *J* = 9.2 Hz, 1H), 6.77 (d, *J* = 7.6 Hz, 1H), 3.98 (s, 3H), 3.04 (t, *J* = 4.4 Hz, 4H), 2.59 (s, 4H), 2.34 (s, 3H); <sup>13</sup>C NMR (400 MHz, Acetone-*d*<sub>6</sub>) δ 164.06, 155.45, 155.15, 154.70, 148.56, 142.11, 139.47, 132.43, 131.28, 129.42, 128.73, 127.02, 126.97, 125.52, 125.43, 125.15, 123.58, 122.81, 115.34, 114.60, 113.47, 112.39, 110.83, 101.96, 55.17, 55.10, 52.95, 45.36; HRMS (FAB+) *m/z* calcd for C<sub>29</sub>H<sub>29</sub>F<sub>3</sub>N<sub>5</sub>O<sub>2</sub> [M+H]<sup>+</sup>: 536.2273, found: 536.2270.

#### 4.4.12. *N*-(3-((5-Methoxyquinolin-2-yl)amino)phenyl)-4-morpholino-3-(trifluoromethyl)benzamide (**9b**)

Column chromatography was performed using a mixture of hexane-ethyl acetate (2:1, then 1:1 v/v). White solid; yield 74.5%; <sup>1</sup>H NMR (400 MHz, DMSO-*d*<sub>6</sub>) δ 10.39 (s, 1H), 9.49 (s, 1H), 8.49 (s, 1H), 8.28–8.24 (m, 3H), 7.84–7.81 (m, 1H), 7.68 (d, *J* = 4.5 Hz, 1H), 7.51 (t, *J* = 8.1 Hz, 1H), 7.36–7.31 (m, 3H), 7.07 (d, *J* = 9.1 Hz, 1H), 6.80 (d, *J* = 7.8 Hz, 1H), 3.95 (s, 3H), 3.76 (t, *J* = 4.0 Hz, 4H), 2.98 (t, *J* = 4.2 Hz, 4H); <sup>13</sup>C NMR (100 MHz, DMSO-*d*<sub>6</sub>) δ 164.36, 155.40, 154.90, 154.83, 148.38, 142.14, 139.59, 133.46, 131.53, 130.00, 129.09, 127.46, 127.40, 125.03, 124.74, 124.33, 119.53, 115.08, 114.70, 114.04, 113.31, 111.31, 102.66, 66.91, 56.08, 53.61; HRMS (FAB+) *m/z* calcd for C<sub>28</sub>H<sub>26</sub>F<sub>3</sub>N<sub>4</sub>O<sub>3</sub> [M+H]<sup>+</sup>: 523.1957, found: 523.1953.

#### 4.4.13. 3-(4-Ethylpiperazin-1-yl)-*N*-(3-((5-methoxyquinolin-2-yl)amino)phenyl)-5-(trifluoromethyl)benzamide (**9c**)

Column chromatography was performed using 0–50% hexane in ethyl acetate. White solid; yield 59.3%; <sup>1</sup>H NMR (400 MHz, CDCl<sub>3</sub>) δ 8.48 (s, 1H), 8.28 (d, *J* = 9.1 Hz, 1H), 8.01 (s, 1H), 7.56 (s, 1H), 7.48–7.42 (m, 3H), 7.38 (d, *J* = 8.4 Hz, 1H), 7.31–7.26 (m, 2H), 7.18 (s, 1H), 6.90 (d, *J* = 9.1 Hz, 1H), 6.65 (d, *J* = 7.4 Hz, 1H), 3.95 (s, 3H), 3.27

(t,  $J = 5.1$  Hz, 4H), 2.56 (t,  $J = 5.0$  Hz, 4H), 2.47 (q,  $J = 7.2$  Hz, 2H), 1.13 (t,  $J = 7.2$  Hz, 3H);  $^{13}\text{C}$  NMR (100 MHz,  $\text{CDCl}_3$ )  $\delta$  165.40, 155.42, 154.31, 151.49, 148.12, 140.95, 138.44, 136.70, 132.56, 131.87, 131.55, 129.86, 129.60, 123.90 (q,  $J = 271$  Hz), 118.92, 117.25, 116.40, 115.81, 114.92, 114.26, 113.21, 112.16, 111.00, 102.07, 55.56, 52.32, 52.23, 47.93, 11.83; HRMS (FAB+)  $m/z$  calcd for  $\text{C}_{30}\text{H}_{31}\text{F}_3\text{N}_5\text{O}_2$   $[\text{M}+\text{H}]^+$ : 550.2430, found: 550.2431.

#### 4.4.14. *N*-(3-((5-Methoxyquinolin-2-yl)amino)phenyl)-3-morpholino-5-(trifluoromethyl)benzamide (**9d**)

Column chromatography was performed using a mixture of hexane-ethyl acetate (2:1, then 1:1 v/v). White solid; yield 72.7%;  $^1\text{H}$  NMR (400 MHz,  $\text{DMSO}-d_6$ )  $\delta$  10.38 (s, 1H), 9.50 (s, 1H), 8.47 (s, 1H), 8.26 (d,  $J = 9.2$  Hz, 1H), 7.85 (d,  $J = 7.2$  Hz, 1H), 7.76 (s, 1H), 7.68 (s, 1H), 7.51 (t,  $J = 8.0$  Hz, 1H), 7.41 (s, 1H), 7.35–7.29 (m, 3H), 7.07 (d,  $J = 9.1$  Hz, 1H), 6.80 (d,  $J = 7.8$  Hz, 1H), 3.95 (s, 3H), 3.80 (t,  $J = 4.4$  Hz, 4H), 3.33 (t,  $J = 4.24$  Hz, 4H);  $^{13}\text{C}$  NMR (100 MHz,  $\text{DMSO}-d_6$ )  $\delta$  164.98, 155.39, 154.89, 151.90, 148.38, 142.15, 139.47, 137.47, 131.44, 130.74, 130.02, 129.09, 119.52, 117.73, 115.09, 114.82, 114.50, 114.26, 113.77, 113.30, 111.53, 102.66, 66.37, 56.08, 48.19; HRMS (FAB+)  $m/z$  calcd for  $\text{C}_{28}\text{H}_{26}\text{F}_3\text{N}_4\text{O}_3$   $[\text{M}+\text{H}]^+$ : 523.1957, found: 523.1955.

#### 4.4.15. *N*-(3-((5-Methoxyquinolin-2-yl)amino)phenyl)-3-(4-methyl-1*H*-imidazol-1-yl)-5-(trifluoromethyl)benzamide (**9e**)

Column chromatography was performed using a mixture of hexane-ethyl acetate (1:1, then 1:2 v/v). White solid; yield 48.7%;  $^1\text{H}$  NMR (400 MHz,  $\text{Acetone}-d_6$ )  $\delta$  10.04 (s, 1H), 8.78 (s, 1H), 8.70 (s, 1H), 8.47 (s, 1H), 8.30 (d,  $J = 9.2$  Hz, 2H), 8.25 (s, 1H), 8.13 (s, 1H), 7.83 (d,  $J = 8.0$  Hz, 1H), 7.54 (s, 1H), 7.50–7.46 (m, 2H), 7.39–7.31 (m, 2H), 7.06 (d,  $J = 8.8$  Hz, 1H), 6.77 (d,  $J = 7.6$  Hz, 1H), 3.98 (s, 3H), 2.22 (s, 3H);  $^{13}\text{C}$  NMR (100 MHz,  $\text{Acetone}-d_6$ )  $\delta$  163.31, 155.44, 154.67, 148.51, 142.19, 139.86, 139.18, 138.50, 138.33, 135.05, 131.45 (q,  $J = 33$  Hz), 129.43, 128.78, 125.01, 122.81, 122.31, 122.15, 119.47, 119.32, 115.33, 114.84, 114.22, 113.43, 112.40, 110.79, 101.98, 55.16, 12.91; HRMS (FAB+)  $m/z$  calcd for  $\text{C}_{28}\text{H}_{23}\text{F}_3\text{N}_5\text{O}_2$   $[\text{M}+\text{H}]^+$ : 518.1804, found: 518.1801.

### 4.5. *In vitro* cell based evaluations

#### 4.5.1. NCI cancer cell screening

The anticancer activity assessment of the selected final compounds over a panel of 60 human cancer cell lines was applied using the sulforhodamine B (SRB) assay at the National Cancer Institute (NCI), Bethesda, Maryland, USA adopting the standard protocol [57].

#### 4.5.2. Cytotoxicity test against L132 and Vero normal cells

L132 (human embryonic pulmonary epithelial cells) and Vero (adult green monkey kidney cells) were maintained in DMEM supplemented with 10% fetal bovine serum (FBS), penicillin (100 units/mL) and streptomycin (100  $\mu\text{g}/\text{mL}$ ). The cells ( $5 \times 10^4$  cells/mL) were seeded into 96-well Greiner  $\mu\text{Clear}$  flat glass bottom plate. Various concentrations of **9a** and **9c** (3 fold dilutions from 100  $\mu\text{M}$  for 10 serial doses) were added to each well in duplicate, then incubated at 37 °C with 5%  $\text{CO}_2$  for 48 h. Then EZ-Cytox (DoGenBio, republic of Korea) was added to each well and the plate was incubated at 37 °C for 30 min in dark condition. After incubation, the optical absorbance was measured, to detect the cell viability %, using a microplate reader (Flexstation3, Molecular Devices) with a 450 nm wavelength.

#### 4.5.3. Mechanistic cell based investigation

4.5.3.1. *Cell cultures and treatment.* HCT-116 (human colon cancer) cells were maintained in RPMI complete medium supplemented with 10% fetal bovine serum (FBS), penicillin (100 units/mL) and

streptomycin (100  $\mu\text{g}/\text{mL}$ ). The cells were incubated in a humidified incubator at 37 °C with 5%  $\text{CO}_2$ . The cells were seeded in the cell culture dishes and treated with compounds **9a** and **9c** at different concentrations for different time points.

4.5.3.2. *Analysis of nuclear morphological changes by Hoechst staining.* Apoptotic nuclear morphology was analyzed using a Hoechst staining according to the manufacturer's instructions. Briefly, cells were seeded in 96 well clear bottom glass plate and treated with compounds **9a** and **9c**. At the end of each experimental period, the cells were treated with the Hoechst (1  $\mu\text{g}/\text{mL}$ ) at 37 °C for 15 min, washed with fresh medium and the fluorescence images were captured by using Leica DMi8 microscope (Wetzlar, Germany).

4.5.3.3. *Flow cytometry analysis of cell cycle induced by compounds 9a and 9c.* The cell cycle was analyzed on HCT-116 cells by treating with **9a** and **9c** at different concentrations for 24 or 48 h. Cells were then trypsinized and the cell suspension was prepared in ice-cold PBS. Then, 70% of ethyl alcohol was added and fixed on ice, followed by centrifugation, washing and resuspended in PBS (250  $\mu\text{L}$ ). RNA was degraded by treating with 100  $\mu\text{g}/\text{mL}$  RNase A (100  $\mu\text{L}$ ) for 30 min at 37 °C. DNA was stained with 50  $\mu\text{g}/\text{mL}$  propidium iodide (200  $\mu\text{L}$ ) for 30 min at 37 °C in dark condition. The cell cycle was analyzed by flow cytometry using BD Accuri™ C6 flow cytometer (BD Biosciences, Franklin Lakes, NJ, USA) by recording 10,000 cells of each sample.

4.5.3.4. *Apoptosis analysis by annexin V and propidium iodide staining.* Cells were plated in 24-well plates and allowed to grow until ~70% of confluency. Then, the cells were treated with compounds **9a** and **9c** (1.25, 2.5 and 5  $\mu\text{M}$ ) for 24 and 48 h. After the incubation period, the medium was aspirated, the cells were gently rinsed with cold phosphate-buffered saline (PBS: pH 7.4). After centrifugation, the cells were resuspended in 200  $\mu\text{L}$  annexin binding buffer (10 mM HEPES, 140 mM NaCl, 2.5 mM  $\text{CaCl}_2$ ; pH 7.4). Then, 5  $\mu\text{L}$  of annexin V Alexa Fluor™ 488 (Thermo Fisher; A13201) and 200  $\mu\text{L}$  propidium iodide from 50  $\mu\text{g}/\text{mL}$  stock (Thermo Fisher; P3566) was added for 30 min on ice in dark condition. An additional 300  $\mu\text{L}$  annexin binding buffer was added, the suspension was mixed gently, and apoptosis was analyzed by flow cytometry using BD Accuri™ C6 flow cytometer (BD Biosciences, Franklin Lakes, NJ, USA) by recording 10,000 cells of each sample.

### 4.6. Tubulin polymerization assay

The fluorescence based *in vitro* tubulin polymerization assay was performed using the tubulin polymerization assay kit (BK006P, Cytoskeleton, USA) according to the manufacturer's protocols. In this assay, tubulin protein (4 mg/mL) was incubated with the indicated concentrations (10  $\mu\text{M}$ ) of compounds **9a**, **9c**, nocodazole, paclitaxel (as positive control), or diluent (0.5% DMSO as negative control) in the general tubulin buffer (80 mM PIPES pH 6.9, 2 mM  $\text{MgCl}_2$ , and 0.5 mM EGTA and 5% glycerol). The polymerization of tubulin was measured by continuously monitoring the absorbance at a wavelength of OD 340 at 30 s intervals (37 °C) over 60 min using the SpectraMAX M3 reader.

### 4.7. *In vitro* kinase screening

Reaction Biology Corp. Kinase HotSpot™ service was used for biochemical evaluations of compounds **8b** and **9a–e** according to the reported assay protocol [13,52].

#### 4.8. Molecular docking

The crystal structure of B-RAF<sup>V600E</sup>, in its DFG-out conformation, with sorafenib was taken from protein data bank (PDB code: 1UWJ) [55]. The homology modeling of C-RAF (Uniprot: p04049) was built from B-RAF<sup>V600E</sup> structure after sequence alignment using Discovery Studio 2020 (DS). C-RAF homology model was selected with the lowest PDF energy. The protein structure of B-RAF<sup>V600E</sup> and C-RAF were prepared for docking by employing protocol (prepare protein) with removing water molecules, and ligands were prepared through protonation at pH 7.4 and energy minimization. The inhibitors were docked into B-RAF<sup>V600E</sup> and C-RAF models using the CDOCKER in DS.

#### Declaration of competing interest

The authors declare that they have no known competing financial interests or personal relationships that could have appeared to influence the work reported in this paper.

#### Acknowledgments

This research was supported by Bio & Medical Technology Development Program (NRF-2019M3E5D4066905) and Korea Research Fellowship Program (NRF-2019H1D3A1A01070882 and 2018H1D3A1A02074556) of the National Research Foundation (NRF) funded by the Korean government (MSIT), and by the Korea Institute of Science and Technology (KIST) Institutional Programs (Grant No. 2E30180 and 2Z05800). This research was also supported by the Korea Institute of Science and Technology Information (KISTI) Institutional Program. We would like to express our sincere gratitude to the National Cancer Institute (NCI, Bethesda, Maryland, USA) for conducting the in vitro anticancer evaluation of the new compounds.

#### Appendix A. Supplementary data

Supplementary data to this article can be found online at <https://doi.org/10.1016/j.ejmech.2020.112756>.

#### References

- [1] World Health Organization, Global Health Observatory, WHO, Geneva, 2018.
- [2] WHO factsheet. <https://www.who.int/news-room/fact-sheets/detail/cancer>, 2018.
- [3] V.T. DeVita, E. Chu, A history of cancer chemotherapy, *Canc. Res.* 68 (2008) 8643–8653.
- [4] M. Vanneman, G. Dranoff, Combining immunotherapy and targeted therapies in cancer treatment, *Nat. Rev. Canc.* 12 (2012) 237–251.
- [5] M.L. Bolognesi, A. Cavalli, Multitarget drug discovery and polypharmacology, *ChemMedChem* 11 (2016) 1190–1192.
- [6] A.K. El-Damasy, N.C. Cho, G. Nam, A.N. Pae, G. Keum, Discovery of a nanomolar multikinase inhibitor (KST016366): a new benzothiazole derivative with remarkable broad-spectrum antiproliferative activity, *ChemMedChem* 11 (2016) 1587–1595.
- [7] J. Das, P. Chen, D. Norris, R. Padmanabha, J. Lin, R.V. Moquin, Z. Shen, L.S. Cook, A.M. Doweiko, S. Pitt, et al., 2-Aminothiazole as a novel kinase inhibitor template. Structure–activity relationship studies toward the discovery of N-(2-chloro-6-methylphenyl)-2-[[6-[4-(2-hydroxyethyl)-1-piperazinyl]]-2-methyl-4-pyrimidinyl amino]-1, 3-thiazole-5-carboxamide (dasatinib, BMS-354825) as a potent pan-Src kinase inhibitor, *J. Med. Chem.* 49 (2006) 6819–6832.
- [8] B.S. Nam, H. Kim, C.-H. Oh, S.H. Lee, S.J. Cho, T.B. Sim, J.-M. Hah, D.J. Kim, J.H. Choi, K.H. Yoo, Aminoquinoline derivatives with antiproliferative activity against melanoma cell line, *Bioorg. Med. Chem. Lett* 19 (2009) 3517–3520.
- [9] W.-K. Choi, M.I. El-Gamal, H.S. Choi, D. Baek, C.-H. Oh, New diarylureas and diarylamides containing 1, 3, 4-triazolopyrazole scaffold: synthesis, antiproliferative evaluation against melanoma cell lines, ERK kinase inhibition, and molecular docking studies, *Eur. J. Med. Chem.* 46 (2011) 5754–5762.
- [10] M. Gao, L. Duan, J. Luo, L. Zhang, X. Lu, Y. Zhang, Z. Zhang, Z. Tu, Y. Xu, X. Ren, Discovery and optimization of 3-(2-(Pyrazolo [1, 5-a] pyrimidin-6-yl) ethynyl) benzamides as novel selective and orally bioavailable discoidin domain receptor 1 (DDR1) inhibitors, *J. Med. Chem.* 56 (2013) 3281–3295.
- [11] Z. Wang, H. Bian, S.G. Bartual, W. Du, J. Luo, H. Zhao, S. Zhang, C. Mo, Y. Zhou, Y. Xu, Structure-based design of tetrahydroisoquinoline-7-carboxamides as selective discoidin domain receptor 1 (DDR1) inhibitors, *J. Med. Chem.* 59 (2016) 5911–5916.
- [12] A.K. El-Damasy, S.H. Seo, N.C. Cho, S.B. Kang, A.N. Pae, K.S. Kim, G. Keum, Design, synthesis, in-vitro antiproliferative activity and kinase profile of new picolinamide based 2-amido and ureido quinoline derivatives, *Eur. J. Med. Chem.* 101 (2015) 754–768.
- [13] A.K. El-Damasy, J.-H. Lee, S.H. Seo, N.-C. Cho, A.N. Pae, G. Keum, Design and synthesis of new potent anticancer benzothiazole amides and ureas featuring pyridylamide moiety and possessing dual B-Raf<sup>V600E</sup> and C-Raf kinase inhibitory activities, *Eur. J. Med. Chem.* 115 (2016) 201–216.
- [14] D. Zhu, H. Huang, D.M. Pinkas, J. Luo, D. Ganguly, A.E. Fox, E. Arner, Q. Xiang, Z.-C. Tu, A.N. Bullock, 2-Amino-2, 3-dihydro-1 H-indene-5-carboxamide-based discoidin domain receptor 1 (DDR1) inhibitors: design, synthesis, and in vivo antipneumatic cancer efficacy, *J. Med. Chem.* 62 (2019) 7431–7444.
- [15] H.-G. Kim, L. Tan, E.L. Weisberg, F. Liu, P. Canning, H.G. Choi, S.A. Ezell, H. Wu, Z. Zhao, J. Wang, Discovery of a potent and selective DDR1 receptor tyrosine kinase inhibitor, *ACS Chem. Biol.* 8 (2013) 2145–2150.
- [16] T. O'Hare, W.C. Shakespeare, X. Zhu, C.A. Eide, V.M. Rivera, F. Wang, L.T. Adrian, T. Zhou, W.-S. Huang, Q. Xu, et al., AP24534, a pan-BCR-ABL inhibitor for chronic myeloid leukemia, potently inhibits the T315I mutant and overcomes mutation-based resistance, *Canc. Cell* 16 (2009) 401–412.
- [17] R. Capdeville, E. Buchdunger, J. Zimmermann, A. Matter, Glivec (STI571, imatinib), a rationally developed, targeted anticancer drug, *Nat. Rev. Drug Discov.* 1 (2002) 493–502.
- [18] A.T. van Oosterom, I. Judson, J. Verweij, S. Stroobants, E.D. di Paola, S. Dimitrijevic, M. Martens, A. Webb, R. Sciot, M. Van Glabbeke, et al., Safety and efficacy of imatinib (STI571) in metastatic gastrointestinal stromal tumours: a phase I study, *Lancet* 358 (2001) 1421–1423.
- [19] G.D. Demetri, M. Von Mehren, C.D. Blanke, A.D. Van den Abbeele, B. Eisenberg, P.J. Roberts, M.C. Heinrich, D.A. Tuveson, S. Singer, M. Janicek, et al., Efficacy and safety of imatinib mesylate in advanced gastrointestinal stromal tumors, *N. Engl. J. Med.* 347 (2002) 472–480.
- [20] X. Liu, A. Kung, B. Malinoski, G.S. Prakash, C. Zhang, Development of alkyne-containing pyrazolopyrimidines to overcome drug resistance of Bcr-Abl kinase, *J. Med. Chem.* 58 (2015) 9228–9237.
- [21] Y. Liu, X. Peng, X. Guan, D. Lu, Y. Xi, S. Jin, H. Chen, L. Zeng, J. Ai, M. Geng, Discovery of novel Ponatinib analogues for reducing KDR activity as potent FGFRs inhibitors, *Eur. J. Med. Chem.* 126 (2017) 122–132.
- [22] M.I. El-Gamal, M.A. Khan, M.S. Abdel-Maksoud, M.M.G. El-Din, C.-H. Oh, A new series of diarylamides possessing quinoline nucleus: synthesis, in vitro anticancer activities, and kinase inhibitory effect, *Eur. J. Med. Chem.* 87 (2014) 484–492.
- [23] D.A. Ibrahim, D.A.A. El Ella, A.M. El-Motwally, R.M. Aly, Molecular design and synthesis of certain new quinoline derivatives having potential anticancer activity, *Eur. J. Med. Chem.* 102 (2015) 115–131.
- [24] Y. Zhou, W. Yan, D. Cao, M. Shao, D. Li, F. Wang, Z. Yang, Y. Chen, L. He, T. Wang, Design, synthesis and biological evaluation of 4-anilinoquinoline derivatives as novel potent tubulin depolymerization agents, *Eur. J. Med. Chem.* 138 (2017) 1114–1125.
- [25] P. Xiang, H. Jie, Y. Zhou, B. Yang, H.-J. Wang, J. Hu, J. Hu, S.-Y. Yang, Y.-L. Zhao, 5-Methoxyquinoline derivatives as a new class of EZH2 inhibitors, *Molecules* 20 (2015) 7620–7636.
- [26] X. Li, C. Wu, X. Lin, X. Cai, L. Liu, G. Luo, Q. You, H. Xiang, Synthesis and biological evaluation of 3-aryl-quinolin derivatives as anti-breast cancer agents targeting ER $\alpha$  and VEGFR-2, *Eur. J. Med. Chem.* 161 (2019) 445–455.
- [27] A.K. El-Damasy, N.C. Cho, A.N. Pae, E.E. Kim, G. Keum, Novel 5-substituted-2-anilinoquinolines with 3-(morpholino or 4-methylpiperazin-1-yl)propoxy moiety as broad spectrum antiproliferative agents: synthesis, cell based assays and kinase screening, *Bioorg. Med. Chem. Lett* 26 (2016) 3307–3312.
- [28] A.K. El-Damasy, S.H. Seo, N.C. Cho, A.N. Pae, E.E. Kim, G. Keum, Design and synthesis of new 2-anilinoquinolines bearing N-methylpicolinamide moiety as potential antiproliferative agents, *Chem. Biol. Drug Des.* 89 (2017) 98–113.
- [29] K. Nepali, S. Sharma, M. Sharma, P. Bedi, K. Dhar, Rational approaches, design strategies, structure activity relationship and mechanistic insights for anticancer hybrids, *Eur. J. Med. Chem.* 77 (2014) 422–487.
- [30] N. Keru, P. Singh, N. Koorbanally, R. Raj, V. Kumar, Recent advances (2015–2016) in anticancer hybrids, *Eur. J. Med. Chem.* 142 (2017) 179–212.
- [31] K. Paul, S. Bindal, V. Luxami, Synthesis of new conjugated coumarin–benzimidazole hybrids and their anticancer activity, *Bioorg. Med. Chem. Lett* 23 (2013) 3667–3672.
- [32] L.K. Gediya, V.C. Njar, Promise and challenges in drug discovery and development of hybrid anticancer drugs, *Exp. Opin. Drug Discov.* 4 (2009) 1099–1111.
- [33] B. Meunier, Hybrid molecules with a dual mode of action: dream or reality? *Acc. Chem. Res.* 41 (2008) 69–77.
- [34] G. Bérubé, An overview of molecular hybrids in drug discovery, *Exp. Opin. Drug Discov.* 11 (2016) 281–305.
- [35] M.-H. Son, J.Y. Kim, E.J. Lim, D.-J. Baek, K. Choi, J.K. Lee, A.N. Pae, S.-J. Min, Y.S. Cho, Synthesis and biological evaluation of 2-(arylethynyl) quinoline derivatives as mGluR5 antagonists for the treatment of neuropathic pain, *Bioorg. Med. Chem. Lett* 23 (2013) 1472–1476.
- [36] NCI website. <https://dtp.cancer.gov/>.

- [37] R.P. Verma, C. Hansch, QSAR modeling of taxane analogues against colon cancer, *Eur. J. Med. Chem.* 45 (2010) 1470–1477.
- [38] I.M. El-Deeb, S.M. Bayoumi, M.A. El-Sherbeny, A.-M. Alaa, Synthesis and antitumor evaluation of novel cyclic arylsulfonylureas: ADME-T and pharmacophore prediction, *Eur. J. Med. Chem.* 45 (2010) 2516–2530.
- [39] A. Elkamhawy, A.N.I. Viswanath, A.N. Pae, H.Y. Kim, J.-C. Heo, W.-K. Park, C.-O. Lee, H. Yang, K.H. Kim, D.-H. Nam, et al., Discovery of potent and selective cytotoxic activity of new quinazoline-ureas against TMZ-resistant glioblastoma multiforme (GBM), *Eur. J. Med. Chem.* 103 (2015) 210–222.
- [40] W.-S. Huang, C.A. Metcalf, R. Sundaramoorthi, Y. Wang, D. Zou, R.M. Thomas, X. Zhu, L. Cai, D. Wen, S. Liu, et al., Discovery of 3-[2-(imidazo [1, 2-b] pyridazin-3-yl) ethynyl]-4-methyl-N-(4-(4-methylpiperazin-1-yl) methyl)-3-(trifluoromethyl) phenyl benzamide (AP24534), a potent, orally active pan-inhibitor of breakpoint cluster region-abelson (BCR-ABL) kinase including the T315I gatekeeper mutant, *J. Med. Chem.* 53 (2010) 4701–4719.
- [41] M.M. Gamal El-Din, M.I. El-Gamal, M.S. Abdel-Maksoud, K.H. Yoo, C.-H. Oh, Design, synthesis, in vitro potent antiproliferative activity, and kinase inhibitory effects of new triarylpyrazole derivatives possessing different heterocycle terminal moieties, *J. Enzym. Inhib. Med. Chem.* 34 (2019) 1534–1543. <https://dtp.cancer.gov/dtpstandard/dwindex/index.jsp>.
- [42] G. Vlahovic, Z. Rabbani, J. Herndon, M. Dewhirst, Z. Vujaskovic, Treatment with Imatinib in NSCLC is associated with decrease of phosphorylated PDGFR- $\beta$  and VEGF expression, decrease in interstitial fluid pressure and improvement of oxygenation, *Brit. J. Canc.* 95 (2006) 1013–1019.
- [43] G. Vlahovic, A. Ponce, Z. Rabbani, F. Salahuddin, L. Zgonjanin, I. Spasojevic, Z. Vujaskovic, M. Dewhirst, Treatment with imatinib improves drug delivery and efficacy in NSCLC xenografts, *Brit. J. Canc.* 97 (2007) 735–740.
- [44] A. Mazzocca, A. Napolitano, M. Silletta, M. Spalato Ceruso, D. Santini, G. Tonini, B. Vincenzi, New frontiers in the medical management of gastrointestinal stromal tumours, *Ther. Adv. Med. Oncol.* 11 (2019) 1–13.
- [45] M.H. Cohen, J.R. Johnson, R. Justice, R. Pazdur, Approval summary: imatinib mesylate for one or three years in the adjuvant treatment of gastrointestinal stromal tumors, *Oncol.* 17 (2012) 300–307.
- [46] E. Raymond, A.A. Brandes, C. Dittrich, P. Fumoleau, B. Coudert, P.M. Clement, M. Frenay, R. Rampling, R. Stupp, J.M. Kros, et al., Phase II study of imatinib in patients with recurrent gliomas of various histologies: a European organisation for research and treatment of cancer brain tumor group study, *J. Clin. Oncol.* 26 (2008) 4659–4665.
- [47] G. Kim, Y.T. Ko, Small molecule tyrosine kinase inhibitors in glioblastoma, *Arch Pharm. Res. (Seoul)* 43 (2020) 385–394.
- [48] A. Shergalis, A. Bankhead, U. Luesakul, N. Muangsin, N. Neamati, Current challenges and opportunities in treating glioblastoma, *Pharmacol. Rev.* 70 (2018) 412–445.
- [49] E.M. Posadas, V. Kwitkowski, H.L. Kotz, V. Espina, L. Minasian, N. Tchabo, A. Premkumar, M.M. Hussain, R. Chang, S.M. Steinberg, et al., A prospective analysis of imatinib-induced c-KIT modulation in ovarian cancer: a phase II clinical study with proteomic profiling, *Cancer* 110 (2007) 309–317.
- [50] D. Matei, R.E. Emerson, J. Schilder, N. Menning, L.A. Baldrige, C.S. Johnson, T. Breen, J. McClean, D. Stephens, C. Whalen, et al., Imatinib mesylate in combination with docetaxel for the treatment of patients with advanced, platinum-resistant ovarian cancer and primary peritoneal carcinomatosis: a Hoosier Oncology Group trial, *Cancer* 113 (2008) 723–732.
- [51] Reaction Biology corporation, Available from: [http://www.reactionbiology.com/webapps/site/Kinase\\_Assay\\_Protocol.aspx](http://www.reactionbiology.com/webapps/site/Kinase_Assay_Protocol.aspx). (Accessed 10 June 2020).
- [52] H. Oka, Y. Chatani, R. Hoshino, O. Ogawa, Y. Kakehi, T. Terachi, Y. Okada, M. Kawaichi, M. Kohno, O. Yoshida, Constitutive activation of mitogen-activated protein (MAP) kinases in human renal cell carcinoma, *Canc. Res.* 55 (1995) 4182–4187.
- [53] F. McPhillips, P. Mullen, B. Monia, A. Ritchie, F. Dorr, J. Smyth, S. Langdon, Association of c-Raf expression with survival and its targeting with antisense oligonucleotides in ovarian cancer, *Br. J. Canc.* 85 (2001) 1753–1758.
- [54] P.T. Wan, M.J. Garnett, S.M. Roe, S. Lee, D. Niculescu-Duvaz, V.M. Good, C.G. Project, C.M. Jones, C.J. Marshall, C.J. Springer, et al., Mechanism of activation of the RAF-ERK signaling pathway by oncogenic mutations of B-RAF, *Cell* 116 (2004) 855–867.
- [55] P. Xie, C. Streu, J. Qin, H. Bregman, N. Pagano, E. Meggers, R. Marmorstein, The crystal structure of BRAF in complex with an organoruthenium inhibitor reveals a mechanism for inhibition of an active form of BRAF kinase, *Biochemistry* 48 (2009) 5187–5198.
- [56] DTP human tumor cell line screen process, Available from: [https://dtp.cancer.gov/discovery\\_development/nci-60/methodology.htm](https://dtp.cancer.gov/discovery_development/nci-60/methodology.htm). (Accessed 10 June 2020).